

Studies of Metal Fires

Project Number: GTSA07

Study of Sodium Spray Fires for Sandia National Laboratories

A Major Qualifying Project Report

Submitted to the Faculty of the

WORCESTER POLYTECHNIC INSTITUTE

in partial fulfillment of the requirements for the

Degree of Bachelor of Science

in Mechanical Engineering

by

Robert Accosta

raccosta@wpi.edu

Laura Archer

larcher@wpi.edu

Date: February 22, 2008

Approved:

Prof. Gretar Tryggvason, Major Advisor

Keywords

1. Metal fires
2. Spray combustion
3. Experimental design

Acknowledgements

Our project would not have been possible without the help and support of many individuals, including our advisor Professor Tryggvason, our liaison Tara J. Olivier, and the Sandia National Laboratories staff. Our advisor provided us with guidance and insight throughout the project, especially when presented with technical problems. Our liaison provided us with continuous feedback and suggestions for project improvements, as well as motivation and guidance. We would also like to thank Thomas K. Blanchat, Jeffrey J. Danneels, John C. Hewson, and Steven P. Nowlen who provided us with a clear understanding of the project goals and tasks. We are grateful for the help, hospitality, and guidance of all who aided in the development of this project.

Abstract

Liquid sodium will be used as a coolant in next generation nuclear reactors. Because sodium exhibits potentially dangerous properties, it is important to understand possible accident scenarios. This project explored the variables which could affect sodium spray combustion, heat flux to a target, and aerosol production. A preliminary design for bench scale experiments was also created. Sandia National Laboratories will use this data to improve computer modeling codes in order to more accurately predict sodium spray combustion.

Table of Contents

Acknowledgements.....	ii
Abstract.....	iii
Table of Contents.....	iv
List of Figures.....	vi
List of Tables.....	vii
List of Equations.....	viii
Executive Summary.....	ix
1. Introduction.....	- 1 -
2. Background Research.....	- 3 -
2.1. Sodium Fast Cooled Reactors.....	- 3 -
2.2. The Importance of Sodium Fires.....	- 5 -
2.3. The Combustion of Sodium.....	- 7 -
2.3.1. Properties of Sodium.....	- 7 -
2.3.2. Reactions.....	- 7 -
2.3.3. Pool Fires.....	- 9 -
2.3.4. Aerosols.....	- 12 -
2.3.5. Spray Fires.....	- 12 -
2.4. Computer Model Development.....	- 13 -
3. Spray Fires.....	- 16 -
3.1. Theoretical Combustion.....	- 16 -
3.1.1. Single Droplet Combustion.....	- 16 -
3.1.2. Spray Fires.....	- 18 -
3.2. Experimental Combustion.....	- 19 -
3.2.1. Single Droplet Experiments.....	- 19 -
3.2.2. Maximum Pressure Based on Oxygen Concentration.....	- 22 -
3.2.3. Upright Nozzles.....	- 23 -
3.2.4. Previous Experiments Postulating Realistic Leaks.....	- 25 -
3.2.5. Previous Experiments Conclusions.....	- 26 -
3.3. Modeling Drop Size Distributions in Atomized Jets.....	- 27 -
3.4. Sodium Burn Rate.....	- 28 -
4. Preliminary Experiment Design.....	- 32 -
4.1. Design Assumptions.....	- 32 -
4.2. Experiment Overview.....	- 32 -
4.3. Scenario Leak Flow Calculations.....	- 35 -
4.3.1. Sodium Flow from a Nozzle as Compared to Water.....	- 41 -
4.3.2. Sodium Droplet Diameter as Compared to Water.....	- 43 -
4.4. Spray Formation.....	- 45 -
4.5. Necessary Nozzle Height for Complete Burning.....	- 49 -
4.6. Nozzle Selection.....	- 54 -
4.7. Measurement Techniques.....	- 59 -
4.8. Cleanup Procedures.....	- 60 -
5. Conclusions and Recommendations.....	- 62 -
References.....	- 65 -
Appendix A: Scaling Droplet Size Tables.....	- 69 -

Appendix B: Required Height for Complete Burn	- 70 -
Appendix C: Nozzle Comparison to Scenarios	- 76 -
Appendix D: Presentation to SNL	- 79 -
Appendix E: Breakdown of Contributions	- 95 -

List of Figures

Figure 1: Compact Loop SFR Power Plant System.....	- 4 -
Figure 2: Pool Layout SFR Power Plant System.....	- 4 -
Figure 3: Regions of Burning Droplet.....	- 17 -
Figure 4: Burning Stages of Sodium in Air.....	- 20 -
Figure 5: Fraction of Sodium Burned.....	- 21 -
Figure 6: Pressure and Temperature Changes.....	- 25 -
Figure 7: Postulated and Realistic Leak Flows.....	- 26 -
Figure 8: Burn rate under free convection limited by heat transfer.....	- 29 -
Figure 9: Burn rate under free convection.....	- 29 -
Figure 10: Mass Transfer between Ambient Oxygen and Flame.....	- 30 -
Figure 11: Surtsey Vessel.....	- 34 -
Figure 12: SNL Experimental Setup.....	- 35 -
Figure 13: Depiction of Pipe Flow.....	- 36 -
Figure 14: Scenario A Leak Flow Rate.....	- 39 -
Figure 15: Scenario B Leak Flow Rate.....	- 40 -
Figure 16: Scenario C Leak Flow Rate.....	- 40 -
Figure 17: Spray Droplet Control Volume.....	- 44 -
Figure 18: Breakup Regimes.....	- 46 -
Figure 19: Three Scenarios Required Height.....	- 52 -
Figure 20: 500 °C Sodium Required Height at various Velocities.....	- 53 -
Figure 21: Flan Fan Nozzle and Spray.....	- 55 -
Figure 22: Full Cone Nozzle and Spray.....	- 55 -
Figure 23: Hollow Cone Nozzle and Spray.....	- 56 -
Figure 24: Vaneless Hollow Cone Nozzle and Spray.....	- 56 -
Figure 25: Twin Fluid Atomization Nozzle with Flat Fan Spray Pattern.....	- 57 -
Figure 26 Phase Doppler Particle Analyzer.....	- 60 -

List of Tables

Table 1: Properties of Liquid Sodium.....	- 7 -
Table 2: Nozzle Configurations for FAUNA test.....	- 24 -
Table 3: Scenario Constants.....	- 38 -
Table 4: Velocity out of Hole Results.....	- 38 -
Table 5: Flow Rate Results.....	- 39 -
Table 6: Densities, Specific Gravity, and Conversion Factors.....	- 42 -
Table 7: Flow Rate Conversion Results.....	- 43 -
Table 8: Properties of Sodium and Water.....	- 43 -
Table 9: Input Values for Weber Equation.....	- 48 -
Table 10: Results of Jet Radius Calculations.....	- 48 -
Table 11: Weber Number Results.....	- 49 -
Table 12: Required Height Scenario Specifications.....	- 51 -
Table 13: Scenario A Required Height.....	- 51 -
Table 14: Scenario B Required Height.....	- 51 -
Table 15: Scenario C Required Height.....	- 52 -
Table 16: 500 °C Sodium Required Height at various Velocities.....	- 53 -
Table 17: Droplet Description and Diameters.....	- 58 -
Table 18: Scaling Droplet Size Calculations for a 50 mm Leak Hole.....	- 69 -
Table 19: Scaling Droplet Size Calculations for a 120 mm Leak Hole.....	- 69 -
Table 20: Required Burn Height Properties at 450 °C.....	- 70 -
Table 21: Required Burn Height with Injection velocity of 1 m/s at 450 °C.....	- 70 -
Table 22: Required Burn Height with Injection velocity of 2 m/s at 450 °C.....	- 70 -
Table 23: Required Burn Height with Injection velocity of 5 m/s at 450 °C.....	- 71 -
Table 24: Required Burn Height with Injection velocity of 8 m/s at 450 °C.....	- 71 -
Table 25: Required Burn Height with Injection velocity of 11 m/s at 450 °C.....	- 71 -
Table 26: Required Burn Height with Injection velocity of 14 m/s at 450 °C.....	- 72 -
Table 27: Required Burn Height with Injection velocity of 17 m/s at 450 °C.....	- 72 -
Table 28: Required Burn Height with Injection velocity of 20 m/s at 450 °C.....	- 72 -
Table 29: Required Burn Height Properties at 500 °C.....	- 73 -
Table 30: Required Burn Height with Injection velocity of 1 m/s at 500 °C.....	- 73 -
Table 31: Required Burn Height with Injection velocity of 2 m/s at 500 °C.....	- 73 -
Table 32: Required Burn Height with Injection velocity of 5 m/s at 500 °C.....	- 74 -
Table 33: Required Burn Height with Injection velocity of 8 m/s at 500 °C.....	- 74 -
Table 34: Required Burn Height with Injection velocity of 11 m/s at 500 °C.....	- 74 -
Table 35: Required Burn Height with Injection velocity of 14 m/s at 500 °C.....	- 75 -
Table 36: Required Burn Height with Injection velocity of 17 m/s at 500 °C.....	- 75 -
Table 37: Required Burn Height with Injection Velocity of 20 m/s at 500 °C.....	- 75 -
Table 38: Nozzle Comparison to Scenario A.....	- 76 -
Table 39: Nozzle Comparison to Scenario B.....	- 77 -
Table 40: Nozzle Comparison to Scenario C.....	- 77 -
Table 41: Summary of Nozzle Comparison.....	- 78 -

List of Equations

Equation 1: Sodium Oxide Reaction.....	- 7 -
Equation 2: Sodium Peroxide Reaction	- 8 -
Equation 3 Sodium Hydroxide Reaction	- 8 -
Equation 4: Energy Equation along a Streamline	- 36 -
Equation 5: Mass Flow Rate	- 36 -
Equation 6: Shortened Energy Equation.....	- 37 -
Equation 7: Enthalpy Equation	- 37 -
Equation 8: Bernoulli Equation	- 37 -
Equation 9: Leak Spray Exit Velocity Equation.....	- 37 -
Equation 10: Volumetric Flow Rate	- 38 -
Equation 11: Specific Gravity.....	- 42 -
Equation 12: Flow Rate Conversion	- 42 -
Equation 13: Surface Tension Force.....	- 44 -
Equation 14: Inertial Force	- 44 -
Equation 15: Balance of Forces	- 44 -
Equation 16: Velocity from Volumetric Flow Rate.....	- 44 -
Equation 17: Radius of Droplet Calculation	- 45 -
Equation 18: Ratio of Droplet Radii	- 45 -
Equation 19: Weber Number of Air.....	- 48 -
Equation 20: Area of Jet	- 48 -
Equation 21: Radius of Jet	- 48 -
Equation 22: Volume of a sphere.....	- 50 -
Equation 23: Density Equation	- 50 -
Equation 24: Time for Complete Droplet Burning.....	- 50 -
Equation 25: Falling Distance for Complete Burn	- 50 -

Executive Summary

The next generation nuclear reactors are being designed to use sodium as a coolant because of its unique properties. However, this could pose a risk for potentially dangerous consequences if sodium were to accidentally leak from the primary or secondary coolant systems. While sodium's properties make it beneficial for cooling, it can cause concrete to dehydrate and crack, as well as react violently with water and oxygen. When sodium is exposed to oxygen in the air it can ignite and combustion may occur. Sodium combustion can occur in many forms, including pool or spray fires. While the characteristics of the fire can differ, any form of a sodium fire could pose negative consequences. Therefore, the technical staff at Sandia National Laboratories (SNL) has postulated possible fire scenarios that may occur. The focus of this project involves the postulated scenario of a spray fire resulting from a leak in the coolant system piping and the potential consequences it can pose.

In order to assess the safety of a reactor design, it can be necessary to have computer codes that accurately model sodium spray fires. There are codes that are currently available; however, a large area for potential expansion of the current models would be to include radiation heat transfer between droplets, radiative flux from the spray fire, and aerosol production rates. With the help of future experimental testing, knowledge and modeling should progress into a better understanding of sodium spray combustion.

Past theoretical and experimental work has been reviewed to understand the combustion of sodium. The experimental work on sodium sprays has shown that oxygen concentration, spray velocity, and spray droplet diameter are a few parameters that could affect sodium spray combustion. This work had also aimed to quantify the burn rate of stationary droplets, droplets subjected to free convection, and free falling droplets. This past work has gathered important results; however, the results are difficult to compare to each other due to the varying test configurations and boundary conditions. It is particularly difficult to compare the results of tests that do not clearly describe these details. Since SNL is interested in the heat flux to a surface and aerosol production caused by a fire, new experiments must be performed to collect this data.

In order to complete these experiments at SNL, a pressure vessel about 10 m high and 3.5 m in diameter will be used to spray sodium from a nozzle in the downward direction. For these experiments, the initial conditions of the sodium and the test vessel must be known. The characteristics of the nozzle and sodium flow are important to determine so that the experimental spray simulates a postulated leak in the coolant system. The height at which the nozzle is placed must also be determined so that complete burning of the sodium spray is achieved.

This report describes the calculations that are recommended to be used as part of the experimental design parameters. The computations were also completed in order to estimate possible characteristics of sodium sprays so that desired results could be acquired from the experiment.

1. Introduction

Generation IV Advanced Burner Reactors will use liquid sodium as its cooling agent. Sodium exhibits desirable heat transfer properties; however, this liquid can pose a great risk if a leak were to occur in the primary or secondary cooling systems. Sodium can be a very reactive metal under particular circumstances and one of its greatest potential risks involves a leak that results in a fire. A sodium fire is of concern because the high temperatures at which sodium burns can have a significant effect on the surrounding environment. The aftermath of a fire could be devastating, even if it is small, especially if system components fail as a result. For this reason, the technical staff at SNL is designing experiments that will help understand the heat flux and aerosol production from potential fires. The focus of this report is on spray fires and will help the technical staff design portions of the experimental setup.

It was necessary to complete a literature review in order to understand the broad range of topics encompassed by this project. Specific areas of concern included the importance of sodium, sodium properties, sodium pool fires, sodium aerosols, computer model development, theoretical sodium combustion, burning rate, and spray characteristics. Spray fires were studied in the most detail to understand past experimental work and potential areas of future experimentation. These previous studies related to the combustion of a falling droplet, the effect of oxygen concentration on the pressure rise in a vessel, upright nozzle spray testing, and simulation of realistic leaks.

Once the literature review had been completed, the preliminary experimental design began. A set of assumptions and general experiment overview, as described by the SNL technical staff, is presented within this report. The calculations for leak flow rate out of various hole sizes are described, including calculations to convert the flow rate of sodium into that of water. Similarly, calculations were completed to compare the diameter of a sodium droplet to a water droplet. Various estimates of the required nozzle height above the bottom of the pressure vessel were formulated based on the specified criteria that all of the sodium shall completely burn before reaching the collection pan. Each of these estimates was calculated based on numerous droplet diameters, which were then used to select the appropriate nozzles for the experiments.

The nozzles were also chosen based on the postulated leak parameters and the calculated leak flow rates. The details and findings from this work are described in the remainder of the report.

2. Background Research

2.1. Sodium Fast Cooled Reactors

The Sodium-Cooled Fast Reactor is a developmental design of a Generation IV nuclear reactor. The goals for the Generation IV reactor are sustainability, safety and reliability, proliferation¹ resistance, and physical protection (U.S. DOE Nuclear, 2002). Another objective in the design is for a closed fuel cycle that will efficiently manage the radioactive elements, known as actinides, and the conversion of fertile uranium.² This system incorporates numerous safety features that are necessary to create a protected environment that includes a long thermal response time, a large gap to coolant boiling, near atmospheric operating pressure of the primary system, and a secondary coolant loop, that acts as a buffer between radioactive sodium in the primary system and the energy conversion system in the power plant (U.S. DOE Nuclear, 2002).

A fuel system that recycles the radioactive elements will produce two different reactor sizes with one of two fuel types. Uranium-plutonium-minor-actinide-zirconium metal alloy fuel produces a smaller power output than uranium-plutonium oxide fuel (U.S. DOE Idaho National Laboratory, 2007). Both of the fuels undergo fission while in contact with free neutrons and consequently produce neutrons. A self sustaining chain reaction results from the neutron production and releases energy at a controlled rate (U.S. Department of Energy Global Nuclear Energy Partnership, 2007).

There are also two types of cooling systems for the nuclear reactor design, the loop type and the pool type, which can be seen in Figure 1 and Figure 2, respectively. Loop type reactors are those in which the primary coolant circulates through the primary heat exchangers outside of the reactor pressure vessel. Pool type reactors are those in which the sodium immerses the primary heat exchangers inside the reactor pressure vessel (U.S. DOE Idaho National Laboratory, 2007). Although sodium exhibits potentially dangerous properties, it will be used as

¹ Spread of information or technology to nations not recognized as having nuclear weapons

² Nuclear fission is the splitting of an atom's nucleus into smaller nuclei.

Fissile material is an element that can sustain a nuclear fission chain reaction.

Fertile material describes nuclides produced by fissile material through neutron absorption and nuclei conversion.

Nuclide is nuclear element distinguished by the amount of protons and neutrons in the atomic nucleus.

a coolant because of its desired heat transfer properties. The following section outlines the possible risks involved with sodium.

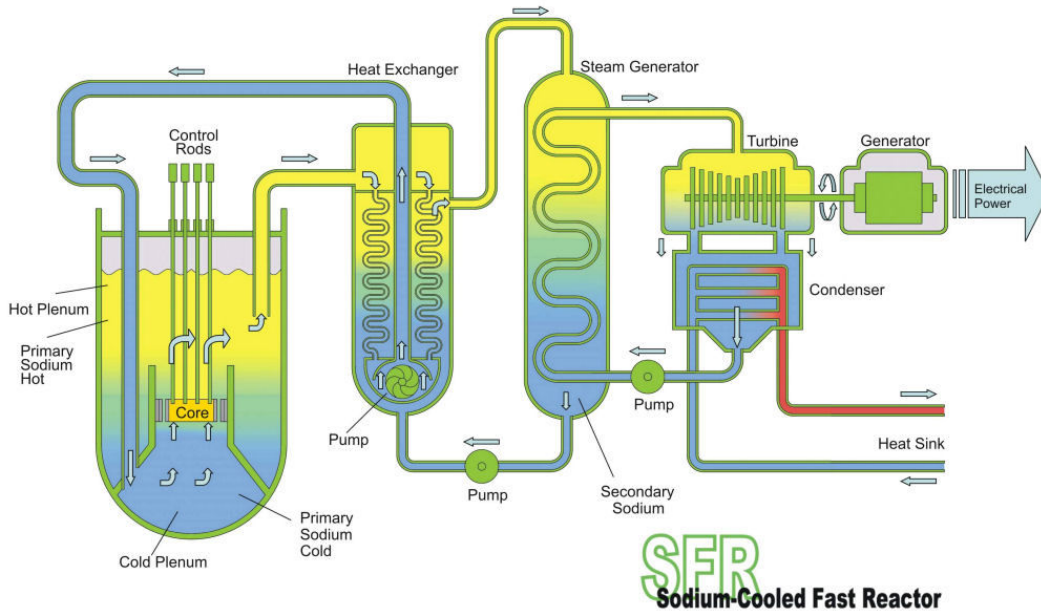


**Figure 1: Compact Loop SFR Power Plant System
(U.S. DOE Idaho National Laboratory)**

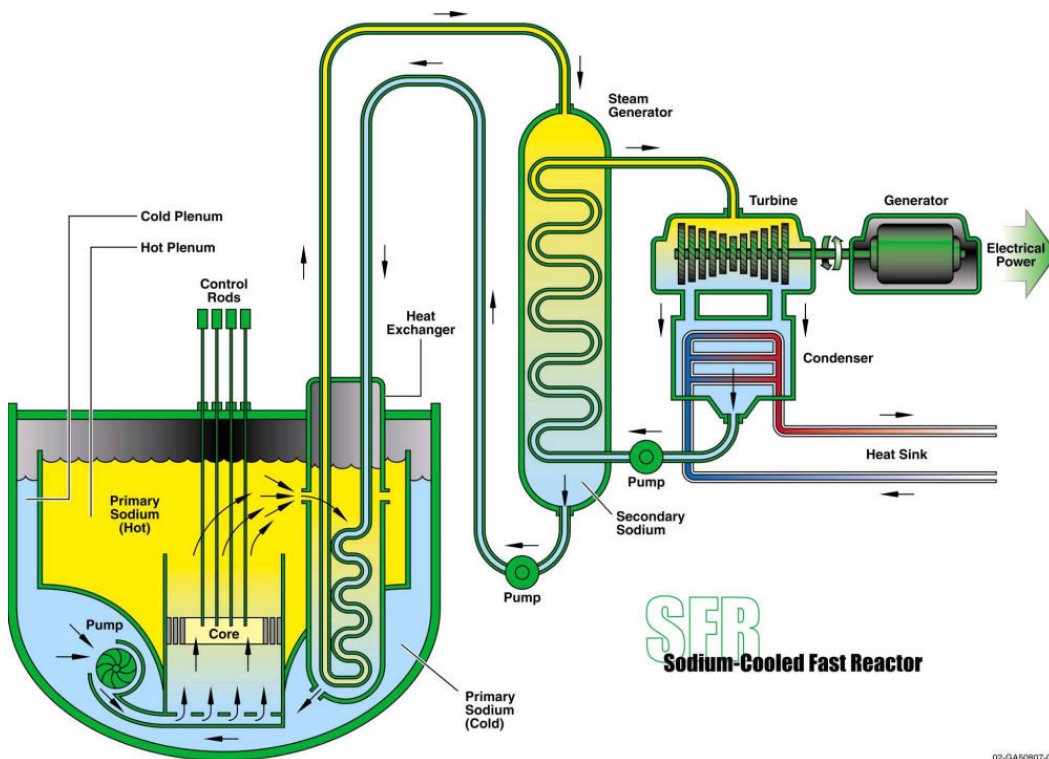


**Figure 2: Pool Layout SFR Power Plant System
(U.S. DOE Idaho National Laboratory)**

02-GA50807-03

2.2. The Importance of Sodium Fires

Even though sodium is beneficial in cooling the reactor, there are potential accident risk scenarios that are still not understood. This section will discuss the potential risks as described by Olivier *et al.*, including radioactive exposure and combustion. These accidents can potentially occur at three times: reactor startup, daily operation, and/or refueling and maintenance. The startup of a reactor could be the most risky procedure because it is unknown if the reactor will function as expected. Since reactor components can be designed separately, unexpected events can occur when each of the components is installed and run within the reactor as a complete system. While every precaution is taken to prevent leaks, it is possible that a design or manufacturing flaw could cause one at this stage.

During the daily operation of the reactor there is the potential for leaks to occur in the heat exchanger, pipeline, valve, reactor vessel, and pumps. While each of these components could potentially leak in different ways, it is extremely important that a leak does not occur. It is possible that even a small leak could cause dangerous consequences. Leaks have the potential to occur because of situations such as defective barriers, thermal loading, ineffective welds, design flaws, seizure of a pump, or sodium induced corrosion. While a leak could potentially cause negative consequences for the plant, it is likely that a break in a component could cause even greater consequences. For this reason, the leak before break concept is exercised in design.

The refueling of a reactor may pose great risks because the processes can be infrequent and complex, as well as have potentially increased consequences if a sodium fire exists. With some equipment, maintenance can be irregular and it could be more likely that procedures will not be followed correctly. Almost all of the incidents described by Olivier *et al.* that led to sodium leaks during maintenance occurred as a result of improper procedure or poor design of procedure.

In each of these cases a sodium leak could cause many consequences, including radioactive exposure, complications with concrete, and fire. If a leak occurred in the primary coolant loop, the sodium could expose nearby personnel to radiation and therefore be potentially unreachable by operators and fire department personnel. Although this is not likely in most

situations because of the many safety procedures used, if such a leak were to reach outside of the plant it could present a health hazard for the general public. Also, if a leak were to occur in a location where the sodium could come in contact with concrete, there could be an impact on the plant's concrete walls, floors, and foundation (Olivier *et al.*, 2007). When concrete interacts with sodium, the concrete exhibits chemical instability that can result in dehydration and cracking (Government of India, 2007). These changes in the material could later result in damage to the plant's foundation and structural failure if a large amount of sodium reacted with the concrete. In addition, Olivier *et al.* explains that if sodium were to leak from the steam generator, cooling of the reactor could diminish. Although loss of coolant is of great concern, the consequences of diminished cooling may not be as great in new generation reactors because cooling will be a natural heat decaying process until the steam generator is repaired (Olivier *et al.*, 2007).

As reviewed in Olivier *et al.*, some of the most dangerous consequences potentially posed by sodium leaks can be those that result in fires because they can cause damage outside of the immediate burn area. A fire at a facility could have serious impacts on the community as the events that occur during the fire may be difficult to overcome. Sodium fires are particularly important because the high temperatures at which sodium burns could cause surrounding components and structures to fail and/or be damaged. Smoke from the incident must be contained in such a way that it does not affect the workers trying to safely shutdown the reactor. For this reason, the placement of the control room and ventilation ducts is of great concern. If the ventilation is not thoughtfully installed, a small incident could result in a large problem if the contaminants are spread throughout the building (Olivier *et al.*, 2007).

Various safety devices and programs have been developed for sodium cooled reactors in an effort to decrease the potential for leaks and/or fires, as Olivier *et al.* explained. These include safe shutdown equipment procedures, administrative efforts to minimize severity, detection and suppression systems, and operating guidelines in the event of a situation. The goal would be to eliminate all possibility of a fire breakout; however, this may not be possible so it is important to understand the causes and consequences so that new innovations can be developed (Olivier *et al.*, 2007).

2.3. The Combustion of Sodium

Olivier *et al.* describes how metal combustion can occur in two different ways, one, if the metals are less volatile than their oxides and, two, if the metals are more volatile than their oxides. For the first case, combustion occurs on the surface of the metal. For the second case, the flame temperatures can increase enough for the vapor pressure to move the reaction off of the metal surface (Olivier *et al.*, 2007). The following sections will explore the properties of sodium, sodium reactions, sodium combustion in the form of pool fires, and aerosol production as a result of sodium fires. Sodium spray fires will also be discussed in this chapter; however, because they are the focus of this report they will be explored in depth in the next chapter.

2.3.1. Properties of Sodium

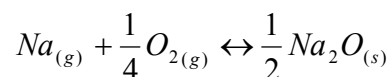
Sodium is a highly reactive alkali metal that can have dangerous consequences. However, for use as a coolant in the next generation nuclear reactors it is a very desirable element because of its heat transfer properties. The ideal property of sodium is its relatively high thermal conductivity as compared to other liquids. Table 1 shows some properties of liquid sodium at various temperatures. The temperatures shown were chosen because leak scenarios were postulated using these temperatures, as seen in section 4.

Temperature (K)	599	606	723	761	773
Density (kg/m ³)	870	870	841	830	829
Specific Heat (kJ/kg K)	1.3	1.3	1.3	1.3	1.3
Kinematic Viscosity *10 ⁷ (m ² /s)	4.0	3.9	3.0	2.9	2.9
Thermal Conductivity (W/m K)	75	74	69	68	67
Thermal Diffusivity *10 ⁵ (m ² /s)	6.5	6.5	6.4	6.4	6.3

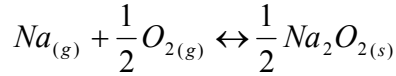
**Table 1: Properties of Liquid Sodium
(Incropera and DeWit, 2002)**

2.3.2. Reactions

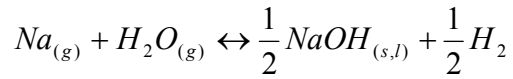
Depending on the sodium combustion chemistry multiple reactions could result, as shown in equations Equation 1, Equation 2, and Equation 3.



**Equation 1: Sodium Oxide Reaction
(Morewitz, 1979,)**



**Equation 2: Sodium Peroxide Reaction
(Morewitz, 1979)**



**Equation 3 Sodium Hydroxide Reaction
(Morewitz, 1979)**

In a fire where there is excess sodium, the monoxide dominates and results in the reaction of Equation 1. However, if air is in excess then peroxide results, as in Equation 2. Equation 3 is not likely to describe a hypothetical fire in the case of a sodium cooled fast reactor because it assumes water vapor as the oxidizer rather than oxygen. All three of these reactions result in fires characterized by very low flames and dense white oxide smoke. This smoke is non-toxic but can cause irritation or damage to ones respiratory organs. The products which do not take the form of smoke form a residue containing sodium oxide and unreacted sodium (Gracie and Droher, 1960). Heat is released during the reaction, which creates a feedback loop that maintains the reaction and increases the temperature of the sodium.

Gracie and Droher describe that the reaction between sodium and any phase of water is very undesirable. This combination results in a very violent reaction, except for when there is no air present and there is enough space for gas expansion. If a mist of water is applied to sodium at very low rates, it will allow the reaction to occur on a small scale. However, if a sufficient amount of water is applied then a violent reaction will result between the heated hydrogen gas in the water and the oxygen in the air. This is an explosive reaction that creates a large noise disturbance (Gracie and Droher, 1960). If the sodium is hot when it comes in contact with water, it may rapidly produce steam in a thermal explosion (Newman *et al.*, 1973). Results from Malet *et al.* tests “showed that humidity inhibits combustion up to 30% relative humidity at 20 °C. This inhibition effect gradually disappears above 60%, but the mean combustion rate does not reach the rate obtained in a dry atmosphere” (Malet *et al.*, 1981).

2.3.3. Pool Fires

A situation in which a sodium leak could become hazardous is in the form of a pool fire. One main factor which determines the ignition of a sodium pool is the oxide layer on its surface, as described by Malet. Depending on how this oxide layer is covering the sodium pool, ignition may not be able to occur. The oxide layer protects the sodium at low temperatures. While the layer is no longer protective at intermediate temperatures, it does not allow oxygen to diffuse through and react with the sodium. At high temperatures, the layer becomes porous and oxidation can occur. If the amount of heat produced from oxidation is greater than the amount of heat lost in the system, ignition will occur (Malet, 1996).

Newman completed experiments to determine the ignition temperature and combustion of sodium pools in an oxygen environment. These experiments focused on static pools of sodium, but also included agitated pools. The static pool experiment included a nickel pot fitted into a well in a 220 watt hot plate heater. A sodium disc with a radius of 2.25 cm and a depth of 6 cm was placed into the nickel pot. Thermocouples were used to monitor and record the temperatures of the nickel pot, heater, and sodium disc. During this experiment there was no attempt made to control the composition of the air, but it was observed that the humidity caused no changes in the ignition behavior of the sodium. Once the experiment was set up, the heater was turned on and three stages of ignition were observed. The first stage occurred at temperatures below 320 °C, when a surface layer of sodium hydroxide was present on the sodium disc and did not allow oxygen to contact the disc. Thus, this surface layer prevented self sustaining reactions from occurring. The second stage occurred at 320 °C, when the sodium ignited and the sodium hydroxide layer became molten. At this temperature, self sustaining surface oxidation occurred and raised the temperature of the sodium disc. Also, yellow areas appeared where monoxide was oxidized to peroxide during this stage. The final stage occurred when the sodium changed from surface oxidation to vapor phase combustion, which was indicated by the onset of flames and smoke production. Since there was a large amount of heat released from the oxide layer, vapor phase combustion occurred (Newman, 1972).

Newman concluded that there are three types of burning within static sodium pools: normal burning, meta stable burning, and vapor phase combustion. The experiments show that

normal burning of static sodium pools is characterized by the presence of smoke and flames, rapid growth, a mean pool temperature of 660 °C, and a 20% release of oxide to the atmosphere. During normal burning, the air oxide interface approaches sodium's boiling point. However, the sodium pool is at a lower temperature because the oxide insulates the pool from the hot region. The second type of burning, meta stable burning, supports flames at temperatures of 600 °C to 700 °C, releases a small amount of oxides to the atmosphere, and is affected by the vapor concentration in the air. This type of burning is characterized by yellow, wispy flames and periodic accumulation of solid oxides on the surface. The last type of burning is vapor phase combustion, which occurs when the sodium pool reaches the metal boiling point. During this type of burning, there are extensive flames, dispersion of sodium on porous materials, oxide release to the atmosphere, and a pool temperature between 800 °C and 900 °C (Newman, 1972).

Newman also conducted an experiment to determine the ignition and combustion of sodium pools which were agitated. For this experiment, 0.1 kg of sodium was placed inside a glass vessel, agitated, and monitored by a thermocouple. The bottom of the glass vessel was heated using electrical resistance while air was allowed to enter the vessel at a rate of 0.5 liter per minute. By completing these experiments, it was concluded that a static pool of sodium will ignite at 320 °C and that an agitated pool will ignite at approximately 150 °C (Newman, 1972). Newman and Payne concluded that because the ignition temperature of sodium (320 °C) is close to the melting point of sodium hydroxide (318 °C), it suggests that the major species in the surface is hydroxide. This surface layer is mechanically broken up by the stirring in the agitated pool experiments, thus allowing oxygen transport and a lower ignition temperature (Newman and Payne, n.d.).

Experiments have also been conducted by Malet *et al.* to understand how sodium temperature and pool area affect the combustion rate. These experiments found that while the initial sodium temperature did not change the mean combustion rate, this rate decreased as the pool area increased. These experiments also found that while the surface area of the sodium affected the burn rate, the pool depth did not (Malet *et al.*, 1981). Other experiments have explored the burn rate and percent consumption of sodium. Johnson *et al.* showed that 90% of 11.3 kg of sodium was consumed in 20 minutes (Johnson *et al.*, 1968). Cherdron and Jordan

recorded an average burning rate for sodium pools to be between 20-40 kg/m²h (Cherdron and Jordan, 1988b).

Further work regarding sodium fires has also been conducted by Newman and Payne, including the areas of smoke generation rates and the chemistry of the vapor phase combustion. This work shows that the smoke produced by sodium combustion is sodium oxide, which is toxic and can lead to serious health hazards when encountered in high concentrations. Through observations of sodium burning between the temperatures of 420 °C and 450 °C, cracks on the surface layer and solid oxide pillars were observed. The formation of these oxide pillars support small regions of flames and white smoke, as well as act as wicks that pull sodium upward and increase the combustion rate. The role of the surface layer was to show that the burning rate does not depend on the surface conditions, but instead on the rate of the mass transfer of oxygen to the reaction zone (Newman and Payne, n.d.).

In order to create experiments similar to a large leak or pipe rupture, Cherdron and Jordan setup large pool fire experiments. The experiments were conducted with pool areas up to 12 m² and 500 kg of sodium. This type of fire can be described in three phases. The first phase occurred during the early minutes of the experiment when there was heating of the above gas layer to high temperatures. The second phase showed a constant temperature that was dependent on the size of the pool and heat transfer properties of the vessel. The last phase was the decline of the high temperatures in the gas layer and the pool of residual sodium (Cherdron and Jordan, 1988b).

Based on the results of the experiments described in this section, it has been found that the ignition of sodium is greatly affected by the oxide layer on the surface of the pool, and that the effects of this layer can be diminished by agitating the pool to break up the layer. These experiments have also found that the combustion rate of sodium is not affected by the initial sodium temperature, but by the combustion area and the rate of mass transfer of oxygen to the reaction zone. The completion of these experiments, and future experiments in this area, are important because they increase the understanding and knowledge of sodium ignition and combustion. This knowledge can then be used to understand the potential risks that the use of sodium may present and how these risks may be minimized.

2.3.4. Aerosols

When sodium reacts with air, the “consequent condensation and coagulation of the reaction products produce large amount of aerosols” (Cherdron and Jordan, 1988a). Cherdron and Jordan describe that these aerosols consist of sodium oxide and their rate of formation is affected by the temperature of the sodium and the rate of oxygen transport to the combustion area. Because sodium pool and spray fires have different burning characteristics, the amount of aerosols formed differs between these types of fires. Experiments have shown that pool fires produce aerosol amounts equal to between 10% and 30% of the burned sodium, while for spray fires this amount is between 30% and 60% of the sprayed sodium (Cherdron and Jordan, 1988a).

The aerosol release rate of spray fires is also dependent on the oxygen concentration, sodium flow rate, and droplet diameter (Cherdron and Jordan, 1988a). These three variables affect the burn rate of the sodium, which then affects the aerosol release rate. The droplet diameter is especially important because a smaller droplet diameter increases the surface area to volume ratio, which allows a greater area of sodium to which oxygen can be transported. This in turn increases the burn rate (Krolikowski, 1968), thus affecting the aerosol release rate.

2.3.5. Spray Fires

Another potentially dangerous situation that could result from a sodium leak is a spray fire. The ignition of sodium sprays depends on the characteristics of the specific event; however, some generalizations can be made. Studies have shown that small sodium particles may ignite at room temperature if they are condensed from a vapor mist (Gracie and Droher, 1960). Ignition at room temperature can occur because “...the surface/volume ratio reaction is high thus allowing for quick temperature increase and entailing ignition” (Malet, 1996). Gracie and Droher show that a temperature of about 121 °C may ignite sodium that is sprayed into the air. The time to ignition is not only dependent on temperature, but could be affected by the droplet size, droplet velocity, and oxygen concentration (Gracie and Droher, 1960).

The combustion rate of sodium spray fires is dependent on the completion of the reaction, energy release rate, burning efficiency, and the oxygen concentration. Testing and previous studies concluded that only a fraction of the sodium is typically reacted, which is important because it affects the heat release rate of the fire (Gracie and Droher, 1960). The burning

efficiency is directly related to the size of the spray droplets and the oxygen concentration. Large falling droplets split into smaller droplets to become stable, thus increasing the burning efficiency (Morewitz *et al.*, 1977). It was determined that lower oxygen concentrations decrease the rate of reaction. At higher concentrations, there is plenty of oxygen to react with the relatively smaller amount of fuel. However, experiments performed by Richard *et al.* verified that burning rates may not vary significantly with a change in mole fraction of oxygen or initial sodium temperature. These results proved that the combustion was controlled by oxygen diffusion (Richard *et al.*, 1969).

Experiments were conducted observing temperatures of falling droplets and it was determined that droplets with a higher surface to mass ratio obtained higher temperatures. Gracie and Droher concluded the highest of these temperatures occurred between 0.05 m and 0.20 m from the nozzle and that the temperatures decreased with an increase in distance away from the nozzle. Similar to the time to ignition, the maximum temperature achieved by a falling droplet was a function of the initial sodium temperature, droplet size, droplet velocity, and oxygen concentration (Gracie and Droher, 1960).

A detailed review of spray fires is included in the following sections. Research focused on current computer modeling codes, comparing past theoretical and experimental work, burn rate, and characterization of droplet size. The study also explored the flow out of a hole in a pipe and its corresponding spray distributions to specific nozzles.

2.4. Computer Model Development

The development of computer codes which model sodium spray and pool fires has been somewhat limited due to the complexity of sodium combustion. As will be discussed, some programs accurately produce results that are partially consistent with experimental work. SOLFAS, SOFIRE-MII, PULSAR, CONTAIN-LMR, Fuego, and VULCAN, are computer models for sodium pool fires, spray fires, or both (Olivier *et al.*, 2007).

SOLFAS is a three dimensional code that uses conservation laws as the governing equations. The code also incorporates sodium pool fires that are represented by a flame sheet

over the pool. “The flame sheet combustion is controlled by the sodium and oxygen supplies by diffusion from the pool surface and turbulent mass transfer from the atmospheric gas, respectively” (Olivier *et al.*, 2007).

SOFIRE-MII is a sodium pool combustion code in which the burning occurs at the pool surface. A limitation of this model is that the combustion rates were assumed to be constant but through experiments it was proved that this rate is affected by the sodium temperature (Olivier *et al.*, 2007).

“PULSAR is a bidimensional code designed to calculate the thermodynamic consequences and the release of aerosols from burning sprayed sodium in confined atmosphere” (Olivier *et al.*, 2007, 36). This code accurately predicts the change in pressure, but does not precisely predict the burn rate. The driving factor to the inaccuracy of the sodium burn rate is the oxygen consumption model. One limitation to this model is that it does not account for radiative heat transfer between sodium droplets because of the theory on which it is based (Olivier *et al.*, 2007).

A model code that describes sodium pool and spray fires is CONTAIN-LMR. This tool encompasses a broader range of accidents that could potentially occur in the nuclear reactor. CONTAIN-LMR is capable, in some situations, of representing the water and sodium aerosols produced during a fire, as well as the interaction between sodium with concrete. A limitation to the program is that it assumes a fixed burning rate which does not take droplet heating into account (Olivier *et al.*, 2007).

The pool and spray fire modeling code Fuego is part of a code suite named Sierra, which “coupled turbulent reacting flow (plus particle transport), radiation transport, and solid heat transfer for comprehensive thermal consequence analysis” (Nowlen *et al.*, n.d.). A very important advantage to this code is that it has been validated (Nowlen *et al.*, n.d.).

VULCAN is a three dimensional fire model that is based on Computational Fluid Dynamics. The code is able to model turbulent combustion, participating media radiation,

reacting droplets, pool fire, and solid combustion (Nowlen *et al.*, n.d.). It also includes a solid model to mesh tool and an “easy to learn graphical user interface [that] facilitates fast learning curve for analysts” (Nowlen *et al.*, n.d.).

While each of these codes is able to model the combustion of sodium by making certain assumptions to simplify the combustion, the results may not always be accurate. For this reason, it is important to complete experiments which will help to explain the complexities of spray combustion. These experimental results will increase understanding of the phenomenon and provide data that can be used to enhance the spray combustion models.

3. Spray Fires

3.1. Theoretical Combustion

The following section reviews past theoretical work that has been completed to quantify and predict the combustion of sprays. Combustion of a spray is complicated to study because of the inter-droplet phenomena associated with it. Therefore, single droplet combustion was investigated initially to understand the basic concepts of spray combustion. The theories of single droplet combustion were then expanded to create spray combustion theories.

3.1.1. Single Droplet Combustion

The combustion of a single droplet can be described using two models that make certain assumptions. The first model presumes that the droplet vaporizes in a hot gas, which simplifies the physical reasoning because mass transfer is not considered. According to Turns, this model assumes that the drop is evaporated in a hot gas and the droplet temperature is equal to the boiling point of the fuel. The hot gas layer surrounding the droplet conducts energy in the form of heat to the surface. Since the droplet is already at its boiling temperature, the energy is directly used to vaporize the fuel. This vaporization rate is equal to the rate at which the mass of the droplet decreases (Turns, 2000).

The second model, presented by Sorbo *et al.*, assumes that a diffusion flame surrounds the droplet before vaporization, thus mass and heat transfer are considered. The model also assumes that during steady burning a single droplet contains various regions. The droplet is first enclosed by a zone that is composed of the vaporized fuel, pyrolyzates, and combustion products. The next layer out from the droplet is a diffusion flame where heat is generated, combustion products formed, and fuel and oxygen are brought together. A visualization of these droplet regions can be seen in Figure 3. The environment bordering the droplet supplies the oxygen and heat for the combustion reaction. Describing combustion in this manner ignores the effects of convection and radiation heat transfer. The model also assumes a non-uniform temperature profile throughout the droplet; however, it assumes uniform pressure (Sorbo *et al.*, 1988).

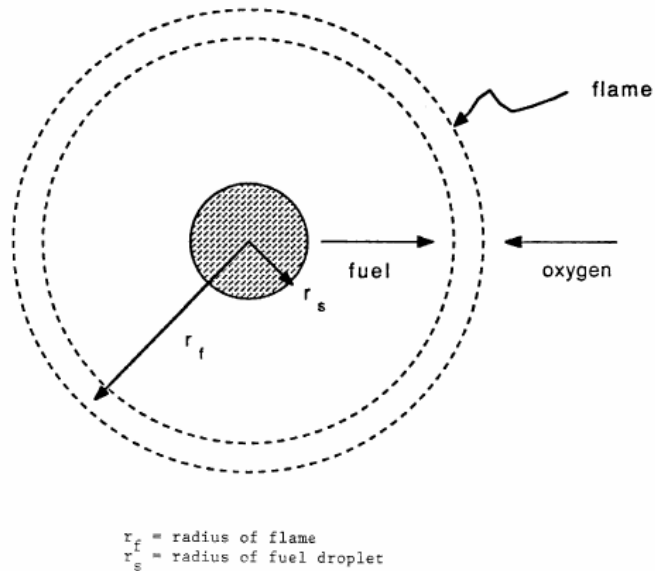


Figure 3: Regions of Burning Droplet (Sorbo *et al.*, 1988)

In Sorbo’s model, the diameter of the droplet is significant because it can be related to the surface area, which determines the amount of area that is available to react with oxygen. “The D^2 -Law is a model which describes the spherically symmetric, isobaric, diffusion-controlled, flame sheet combustion of an isolated, single-component fuel droplet with a constant and uniform droplet surface temperature” (Sorbo *et al.*, 1988). The assumption that “the droplet surface temperature is uniform throughout its lifetime implies that the droplet surface area regression rate, β , is constant and independent of the instantaneous droplet size” (Zung, 1978). The constant regression rate is important because it decreases the amount of surface area available for reaction.

The thickness of the diffusion flame assumed in Sorbo’s model is a function of the chemical reaction rate. Faster reaction rates produce thinner flames while slower rates produce thicker flames. The flame sheet is infinitesimally thin, thus any fuel vapor reacts instantly with the oxygen. All predictions from this burning model are relative to the droplet surface (Sorbo *et al.*, 1988).

The theory behind Sorbo’s model is characterized by the transformation of the liquid droplet to a vapor as the result of a flame engulfing the droplet. Here, heat is conducted through

the gas phase to the surface of the droplet from the flame. The energy is directed towards vaporizing the fuel, while any excess energy is conducted to the interior of the droplet (Sorbo *et al.*,1988). The gasification can only occur in an environment where the temperature and oxygen concentration are ideal for the particular fuel.

3.1.2. Spray Fires

The combustion of a single droplet is the foundation for spray fire burning. Theories of single droplet combustion can be expanded to describe the combustion of a spray. For this reason, Krolkowski developed a model to predict the burning rate and temperature of a single droplet moving through air. This model assumes that there is a combustion zone around the droplet to which oxygen diffuses. It is also assumed that this diffusion of oxygen controls the reaction rate. The mathematical model was then expanded to predict the results of sodium spray combustion (Krolkowski, 1968).

For this spray model, “a quasi-steady-state approach and an averaging technique were used to correlate the reaction rate of individual particles with the theoretical burning rate of a spray and theoretical pressure rise in the enclosed volume” (Krolkowski, 1968). Krolkowski assumed that each droplet in the spray is spherical, of equal size, formed at the nozzle, and distributed evenly over the cross section of the experiment vessel. However, the assumption that the droplets are evenly distributed is not valid for a vessel whose diameter is much larger than that of the nozzle diameter (Krolkowski, 1968). It was also assumed that “ignition of the spray is instantaneous at the point of origin” and “the spray chamber is an adiabatic volume” (Krolkowski, 1968).

As Krolkowski explains, the model split the containment vessel up into numerous vertically stacked sub-volumes. This approach requires that the velocity and the diameter of the droplet be specified because they are the driving factors that influence the burn rate. Additionally, a time period is specified as the amount of time for the droplet to move through a sub-volume. The number of particles that left the nozzle in a time period is calculated. These particles are then represented as one average particle that leaves the nozzle at half of the time period. With use of the pressure, temperature, particle diameter, and composition conditions, the steady state burn rate for each sub-volume is calculated at the start of each time period. The

model can then go on to calculate the heat released and the diameter of the particle after it reacts in the sub-volume. The calculations are repeated until all of the sodium has been sprayed (Krolikowski, 1969).

Using this model, Krolikowski found that the size of the droplets within a spray have the greatest effect on the spray's combustion. As the droplet size decreases, the surface area to volume ratio increases, thus there is more area with which the oxygen can react and the burn rate increases. An increase in the burn rate causes an increase in the pressure rise within the enclosed vessel (Krolikowski, 1968). While the initial sodium velocity and temperature had a very small effect on the reduced pressure-rise rate, "the theoretical reduced pressure-rise rate is inversely proportional to the particle diameter to the 1.47 power" (Krolikowski, 1968).

Spray combustion experiments were also conducted and their results were compared to the theoretical work (Krolikowski, 1968). It was found that "the theory correctly predicted the direction and magnitude of the experimentally observed variations in reaction rate with respect to oxygen content, spray velocity, and particle size" (Krolikowski, 1968). Because the theoretical results agreed with the experimental results, including the reduced pressure-rise rates, the model is considered to be "a good representation of the burning phenomenon" (Krolikowski, 1968).

3.2. Experimental Combustion

While theoretical work has been completed to understand the combustion of a sodium spray fire, experimental results must be obtained to test the accuracy of these theories. The following section will describe various experiments including single droplets, maximum pressure based on oxygen concentration, upright nozzles, and postulated realistic leaks. The experiments were able to verify many qualities and characteristics that sodium exhibits.

3.2.1. Single Droplet Experiments

In order to gain a better understanding of the risk posed by the use of sodium as a coolant, sodium drop burning experiments have been completed. Morewitz *et al.* conducted experiments of sodium combustion of free falling drops. The sodium was first heated to 555 °C and injected out of a circular nozzle to form single drops. Each drop fell 14.7 m into an argon filled collecting tank. Once the experiments were complete, the sodium collected in the tank was

dissolved in water. A flame photometer was then used to analyze the mixture of water and dissolved sodium to quantify the sodium content and calculate the average mass of a single droplet (Morewitz *et al.*, 1977).

Morewitz *et al.* also collected data during the experiment by placing a camera with its shutter open, so that as each drop fell past the camera it would leave a vertical streak on the developed film. This streak photography was able to show the three stages the drop completed while falling. The first stage is characterized by no light being present, which indicates no combustion. The second stage shows ignition of the drop when the first light appears. When the width of the light is stable, then full burning of the drop is occurring in the final stage. Figure 4 shows each of the distances from the nozzle at which these three stages occurred based on the initial droplet diameter (Morewitz *et al.*, 1977).

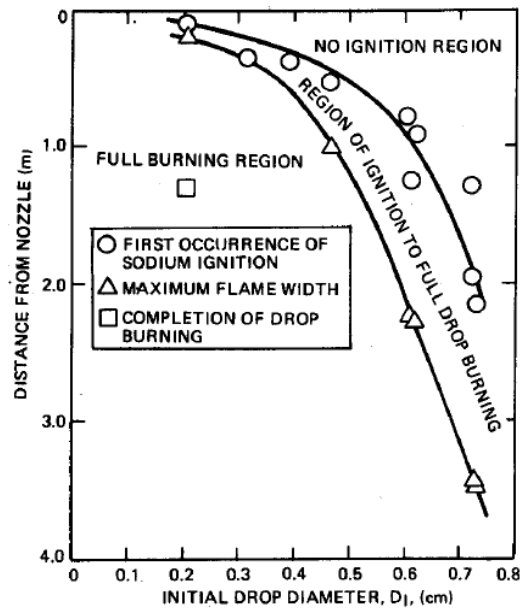


Figure 4: Burning Stages of Sodium in Air (Morewitz *et al.*, 1977)

Morewitz *et al.* also used the streak photography to conclude that droplets with an initial diameter of approximately 0.93 cm were nearly spherical at formation. Later, protrusions were formed on the drop that then shed off and created satellite drops of approximately 0.2 cm in diameter. The original droplet continued to fall and burn until it was collected in the tank, while the satellite drops ignited after falling about 10 cm. The satellite drops were completely burned

after 1.3 meters. It was found that these larger drops continued to shed satellite drops until they reached a stable diameter of 0.7 cm. The streak photography was used to conclude that drops with a diameter less than 0.3 cm burned completely within falling 1.3 m from the nozzle. The images also showed that all drops greater than or equal to 0.3 cm in diameter did not completely burn before they reached the collection tank. Figure 5 shows the fraction of sodium burned based on the initial drop diameter. From this figure it can be seen that for drops with an initial diameter of 0.3 cm to 0.8 cm the fraction of sodium burned is inversely proportional to the initial drop diameter. These results show the shortcomings of models which only use average drop sizes to calculate the burning of sodium sprays (Morewitz *et al.*, 1977). Instead, models must “account for the complete local combustion of large numbers of small drops, and for the maximum size of the large drops” since this combination of large and small drops increases the amount of sodium burned within a spray (Morewitz *et al.*, 1977).

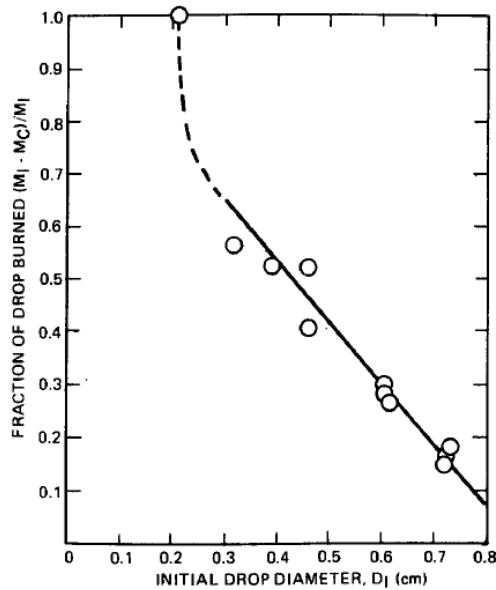


Figure 5: Fraction of Sodium Burned
(Morewitz *et al.*, 1977)

Rockwell International performed numerous experiments with single droplets to study the burning characteristics of sodium, particularly burn rate, in their Laboratory Drop Modeling test apparatus. This device is a 30 cm diameter pipe that is 1.8 m long. The first of the tests consisted of numerous stationary sodium droplet burning trials. It was determined that the burn rate was independent of the humidity level; however, there was a dramatic difference between burn rates

under natural and forced convection (Rockwell International, 1975). The tests concluded that “the burning rate increased by a factor of 40” when a droplet was subjected to forced convection as compared to free convection (Rockwell International, 1975).

A sodium falling droplet test was also performed by Rockwell International in the same apparatus with an oxygen concentration of 21%. Droplets that were pre-heated to 430 °C to 480 °C fell from both 3.9 m and 5.5 m. Still photography was used to determine that the average initial diameter of each droplet was 0.76 cm. Streak photography was also used for the determination that the droplets ignited after falling 0.6 m and were fully burned at 2.5 m below the release point. The conclusion of the falling droplet tests was that “the burning rate of sodium in 21 vol % O₂ was 170 mg/sec” (Rockwell International, 1975).

These experiments of single droplets provided data regarding the burning characteristics of sodium. However, these characteristics may be affected by events that take place within a spray. It is also important to conduct experiments that explore the effects of these events, particularly radiative heating between droplets and oxygen penetration into the spray.

3.2.2. Maximum Pressure Based on Oxygen Concentration

As discussed previously, the availability of oxygen to the sodium may affect its burning characteristics. For this reason, various experiments have been conducted to test the effects of varying oxygen concentration. The pressure rise in the test vessels was specifically recorded as it is an indication of the reaction rate, thus it may be possible to draw conclusions from the pressure data.

A set of experiments conducted by Krolkowski used a vessel that was 0.91 m long and 0.15 m in diameter to create an environment with varying oxygen concentrations. A fixed amount of sodium was sprayed through nozzles with diameters varying between 0.25 mm and 0.76 mm. The purpose of measuring the different pressure rise rates was because it can be used as a gauge of the reaction rate. This experiment resulted in a mean droplet diameter of 420 μm and unburned sodium left on the walls of the vessel. A maximum pressure rise and rate of rise of 4.15 bar and 76 bar/sec, respectively, were obtained. It was concluded that “the only effective

difference between the explosive ejection and the pressurized spray of sodium is the reaction rate” (Krolikowski, 1968).

Hines *et al.* conducted experiments in a small vessel having a diameter of 0.76 m and a length of 1.25 m. The purpose of these tests was to determine the effect of oxygen concentration on the pressure rise in the vessel. An oil-burner nozzle was used to spray the 455 °C sodium into the vessel. A maximum pressure of 3.7 bar was obtained at 21 vol % oxygen. The results from the testing proved that as the initial oxygen concentration decreased, the maximum pressure in the vessel also decreased (Hines *et al.*, 1956).

3.2.3. Upright Nozzles

In order gain a better understanding of spray combustion and the variables that could affect it, various experiments were conducted using upright nozzles. The exact nozzle configuration varied between experiments, but all experiments used nozzles that sprayed sodium upward.

The following spray tests were conducted by Cherdron and Jordan in the FAUNA vessel, which was 6 m in height and 6 m in diameter. The tests studied the influence of the sodium conditions, as well as the geometry, shape, size, and location of the leak. The FAUNA containment structure could spray sodium in an upward manner with several different nozzles configurations. Possible nozzles included those with multiple holes ranging from one to several. Each hole had a diameter of 26 mm or less. The second type of nozzle had a square slit that was 1 mm wide and 50 mm long. The flow rate ranged from 0.5 kg/sec to 56 kg/sec depending on the test. The peak temperature for this particular experiment was 800 °C (Cherdron and Jordan, 1988b). “The overpressure peak value can be related to the spray flow rate and design of the nozzle used” (Cherdron and Jordan, 1988b, 4). The overpressure is defined as the pressure rise above the initial pressure.

The FAUNA facility was also used for other experiments in which circular and slit nozzles sprayed sodium. The nozzles were directed upward and were supplied with sodium by an argon supply tank at 10 bar (Cherdron, 1986). The Cherdron test setup also contained a device that kept

the pressure gradient constant between the argon tank and the vessel as the experiment was carried out. The different nozzles used in this test can be seen in Table 2.

Nozzle	Description
1	1 hole, 8 mm diam.
2	4 holes, 4 mm diam. each
3	1 square slit 1 x 50 mm ²
4	1 square slit 4 x 12, 5 mm ²
5	1 rough edged slit, 50 mm ²
6	64 holes, 1 mm diam. each
7	8 holes, 4 mm diam. each
8	6 holes, 8 mm diam. each

Table 2: Nozzle Configurations for FAUNA test (Cherdron, 1986)

The sodium flow rate, total amount of sodium burned, and shape of the nozzle were the variables of the experiment. The test resulted in different pressure increases in the vessel for different nozzles. The overpressure for nozzles one through five did not exceed 1 bar, suggesting that these nozzles produced sprays with low burning efficiencies. Nozzles six, seven, and eight all reached above 2 bar, which could have been the result of a higher flow rate (Cherdron, 1986).

In order to understand the burn rate of sodium and the effects of a sodium spray fire on the pressure and temperature in an enclosed vessel, Kawabe *et al.* conducted the following experiment. The vessel chosen was 2.8 m tall, 1 m in diameter, and included a spray nozzle at its base. An amount of 0.4 kg of sodium was heated between 300°C and 530 °C and sprayed upward into the vessel. The spray lasted about eleven seconds and created the shape of a full, inverted cone. The initial conditions of the vessel were controlled in order to vary the oxygen concentration between the tests. Throughout the experiment the oxygen concentration, pressure, and temperature within the vessel were measured and recorded. Figure 6 shows the change in temperature and pressure over the time period of the experiment.

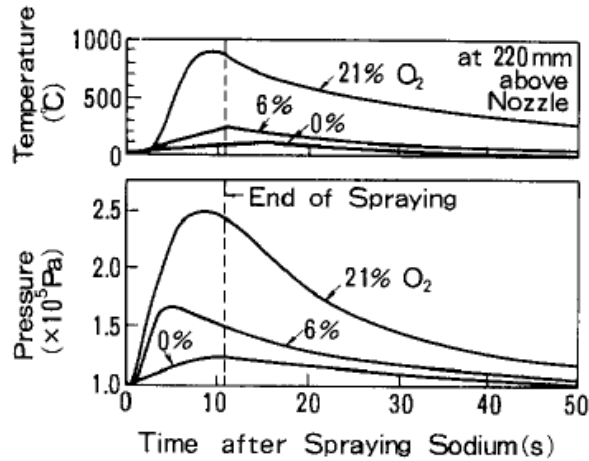


Figure 6: Pressure and Temperature Changes
(Kawabe *et al.*, 1982)

From the figure it can be seen that the pressure and temperature changes were greatly dependent on the initial oxygen concentration. As the initial oxygen concentration was increased, the values of the temperature and pressure also increased (Kawabe *et al.*, 1982). The results showed that “the temperature in the spray outer region was higher than that of inner region and observed oxygen consumption was not more than 80% of that expected for complete combustion of sodium” (Kawabe *et al.*, 1982). This temperature distribution in the spray can be attributed to an uneven distribution of oxygen, and thus combustion, throughout the spray. While oxygen was provided to the spray through convection and diffusion, the inside of the spray received less than the outside (Kawabe *et al.*, 1982).

3.2.4. Previous Experiments Postulating Realistic Leaks

While each of the above experiments was helpful in understanding the combustion of a sodium spray, Himeno conducted experiments designed to simulate a realistic leak. These experiments aimed to understand the effects of a sodium leak in the secondary coolant system of an Advance Breeder Reactor, therefore piping with an inner jacket, thermal insulator, and an outer jacket was used. Himeno also completed spray combustion tests. For each set of experiments, the weight of sodium used ranged from 200 kg to 3 tons at a flow rate of 20 kg/min to 240 kg/min. It was found that the combustion during the realistic leak experiment was less than that of the spray combustion experiment (Himeno, 1988). These results are explained by “...the fact that the inner and outer jackets suppressed generating a spray but just allowed to

generate a downward column leak...” (Himeno, 1988). The postulated and realistic leak flows can be seen in Figure 7.

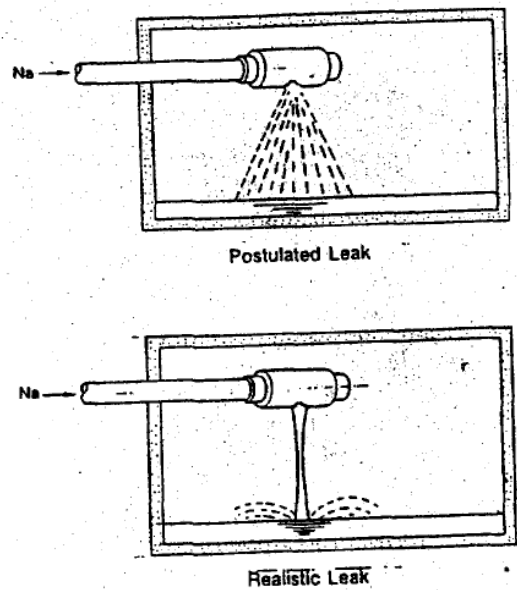


Figure 7: Postulated and Realistic Leak Flows
(Morewitz, 1979)

3.2.5. Previous Experiments Conclusions

Each of the spray experiments explained in this section were conducted using different setups and variables; however, they all attempted to gather new information to measure and understand similar concepts. The single droplet testing concluded that for a small range of droplet sizes the portion of sodium burned was inversely proportional to the diameter. Also, while the burn rate was not affected by the humidity level, there was a large difference between the burn rates of sodium droplets subjected to natural and forced convection. Spray experiments deduced that the burn rate and/or burning efficiency may decrease with a decreasing oxygen concentration. Additionally, pressure and temperature in the test vessel decreased with a decreasing oxygen concentration.

While the experiments were able to verify many characteristics that sodium exhibits, it is difficult to compare the results of the experiments because each experiment used different equipment, initial conditions, and experimental procedures. This difficulty is increased because much of the experimental literature does not include details on the boundary conditions of the

experiments. However, one conclusion that has been made is that “only when ultra fine particles of liquid sodium, produced by explosive injection, are reacted with oxygen do the experimental pressure rises approach those predicted by equilibrium thermodynamics. However, further work is required to understand the detailed behavior of sodium spray fires” (Morewitz, 1979). Since SNL is interested in understanding the particular effects of a fire in relation to the heat flux to a target and aerosol production, experiments will be conducted to gather data in these areas.

3.3. Modeling Drop Size Distributions in Atomized Jets

As can be seen in the past experimental work, the droplet diameter is an important factor in the combustion of sodium sprays. For this reason it is desirable to predict the droplet diameters present in a spray and their distribution throughout it. “Knowledge of the effect of variations in fluid physical properties, atomizer geometry, and atomizer operating parameters on drop size distribution is crucial if control of the resulting distribution is desirable” (Babinsky and Sojka, 2002). Atomization droplet size distributions can be represented by the empirical method, maximum entropy method, or the discrete probability function method (Babinsky and Sojka, 2002).

The empirical method is the only one of the three that is not an analytical approach. Babinsky and Sojka state that for this method a wide range of data is collected for different nozzle configurations and test conditions. The results are then plotted and a curve is fitted to them. The curves that frequently occur over various trials become standard empirical distributions. A drawback of this method is that information is limited to the specific test because results outside of the test conditions cannot be confidently extrapolated. Therefore more experiments must be completed in order to verify the predictions of the extrapolation. Unfortunately, this may not be possible and/or affordable (Babinsky and Sojka, 2002).

Another approach to modeling the drop size distribution is the maximum entropy method. This method “views spray formation as a completely non-deterministic process that can be modeled using the principle of entropy maximization subject to a set of global constraints” (Babinsky and Sojka, 2002). Babinsky and Sojka explain that in order to apply this method the correct constraints must be used. These constraints have been defined to contain source terms

which are expressed as possible diameters in the drop size distribution. In order to predict a drop size distribution at least two diameters must be known. Because it is only possible to predict one of these diameters using analytical methods, the maximum entropy method is not practical (Babinsky and Sojka, 2002).

The last option is the discrete probability function method, which “divides the spray formation process into deterministic and non-deterministic portions. It is assumed that spray formation involves a series of breakup stages of the initial fluid structure” (Babinsky and Sojka, 2002). Formulations by Rayleigh, Weber, and others can be used for an instability analysis that will describe the breakup process. The fluctuation of initial conditions as a result of turbulence, surface roughness, vortex shedding, etc. cause the distributions of drop size. “The drop size distribution is computed by coupling a deterministic model that describes the formation of a single drop to the discrete probability function” (Babinsky and Sojka, 2002). The probability density function is a necessary input for this model. The only downside to this model is that it has not been experimentally verified.

These three options for determining the droplet distribution in a spray are available; however, they are not practical for the purposes of this report because of the disadvantages discussed. If it is critical to know the droplet distribution it should be measured experimentally.

3.4. Sodium Burn Rate

The burn rate of a sodium droplet has been examined as one of the many critical parameters of spray combustion. In order for a burn rate to be measured, the sodium must start “to oxidize sufficiently rapidly [so] that a self-generated temperature rise is produced” (Newman, 1983). This means that a visible flame does not have to be present for ignition. Newman also mentions that there has been a variety of research done to characterize the ignition temperature for sodium, but there are large discrepancies between experts. There have been studies and experiments that measured burn rates for use in predictive models. For the purposes here, only three different spray fire scenarios were evaluated. These situations were the burning of a stationary droplet, burning of droplet subjected to free convection, and burning of a drop under forced convection (Newman, 1983).

The studies determined that the burn rate was slightly affected by variations in initial sodium temperature, particle velocities, and oxygen concentrations greater than 5% (Newman, 1983). The variable that had the largest impact on the burn rate was the spray particle size. Other experimental work proved that sodium's burn time was proportional to the "D² law" (Richard *et al.*, 1969).

Newman in 1983 expresses the burn rate of a stationary sodium droplet that is limited by heat transfer in the following manner:

$$Br = r \left[9.95 * 10^{-2} \left(\frac{T}{573} \right)^{1.75} X_{O_2} - 2.12 * 10^{-3} \right]$$

Figure 8: Burn rate under free convection limited by heat transfer (Newman, 1983)

Where:

Br = Burn rate

r = Droplet radius

X_{O₂} = Mole fraction of oxygen

T = Temperature

Another modified model is one that describes a burning droplet under natural convection. For this method, the assumption needs to be made that forced convection is not present. When considering both mass and heat transfer to the droplet, the burning rate can be determined from the following correlations;

$$B_r = \frac{Sh(D)}{d} C_{mean} (X_{O_2\infty} - X_{O_2flame})$$

$$Sh = 2 + 0.43(Gr)^{1/4} (Sc)^{1/3}$$

Figure 9: Burn rate under free convection (Newman, 1983)

Where:

Br = Burn rate

D = Diffusion coefficient

d = Diameter

C_{mean} = Mean molar concentration

X_{O₂∞} = Ambient mole fraction of oxygen

X_{O₂Flame} = Flame mole fraction of oxygen

Sh = Sherwood number

Gr = Grashof number

Sc = Schmidt number

$$Gr = \frac{d^3 g \beta (T_f - T_\infty)}{\nu}$$

$$Sc = \frac{\nu}{D}$$

B = Volumetric thermal expansion coefficient

T_f = Temperature of the flame

T_∞ = Ambient temperature

ν = Kinematic viscosity

In experiments carried out by Heisler *et al.* (1975 a, b) the burn rates of stationary and falling sodium drops were measured. Stationary drops having a diameter of 7.6 mm produced a burn rate of 7.7×10^{-6} kg/s, while droplets falling from 5.5 m had burn rates of 0.17 mg/s (Heisler *et al.*, 1975b). The falling droplet had a significantly higher burn rate due to the forced convection subjected on the drop. “It was found, that a 2.1 mm diameter droplet ignited after falling 0.1 m and was burning fully after falling 0.2 m, whereas a larger drop 7.2 mm in diameter ignited after 1.2 m and was fully burning after falling between 2 and 3 m” (Heisler *et al.*, 1975a). A burn rate for this falling droplet subjected to forced convection was attained with the use of a numerical solution that incorporated the following mass transfer correlation (Krowlikowski, 1969):

$$Sh = 2 + 0.6 Re^{1/2} Sc^{1/3}$$

Figure 10: Mass Transfer between Ambient Oxygen and Flame
(Newman, 1983)

Where:

Sh = Sherwood number

Re = Reynolds number

Sc = Schmidt number

$$Re = \frac{Vd}{\nu}$$

$$Sc = \frac{\nu}{D}$$

V = Velocity

d = Diameter [m]

ν = Kinematic viscosity

D = Diffusion coefficient

The burn rate model for a droplet subjected to forced convection was compared to theoretical results and this comparison determined that the model was consistent with theoretical results until oxygen concentrations of 15%. If the oxygen concentration was higher than 15%, the model over-predicted the burn rate (Krolikowski, 1969). There are also computer codes available that use numerical methods to formulate a burn rate; however, these codes may not have been extensively validated (Krolikowski, 1969). Experiments have also been completed to quantify the burn rate. For example, the conclusion of the falling droplet tests described in Section 3.2.1 was that “the burning rate of sodium in 21 vol % O₂ was 170 mg/sec” (Rockwell International, 1975). This value for the burn of a falling droplet will be used in following calculations because it is the best estimate available.

4. Preliminary Experiment Design

4.1. Design Assumptions

The participants of the International Atomic Energy Agency's "International Working Group on Fast Reactors Specialist's Meeting on Sodium Fires" used many different approaches to define the worst case leak scenario that should be considered during experiment and plant design. The United Kingdom participants considered the worst leak to occur as a double-ended guillotine of the largest pipe at the worst location possible, while many other participating countries were attempting to adopt a leak before break approach. While the leak before break approach was being developed, many participants were using Moderate Energy Fluid System Approach, which states that the leak area is equal to one fourth of the product of the pipe diameter and the pipe thickness (International Working Group, 1988). Cherdron *et al.* states that "a basic leak area should be regarded at each point of the main piping corresponding to the diameter of the greatest pipe connection of auxiliary systems" (Cherdron *et al.*, 1988). Since the goal of the preliminary experiment is to represent an operational accidental leak, it is important to consider a wide range of hole diameters.

It is not only important to know the size of the hole in the piping, but also how sodium will flow out of it. Antonakas discusses the factors that affect the way sodium flows through a crack. He describes that the flow rate is dependant on the configuration of the crack, the loading applied on the pipe, and the heat insulator in direct contact with the pipe wall (Antonakas, 1988). Since the aim of the experiment design is to test a general case, the exact crack configuration and loading are unknown. It is assumed that the crack will be a circular hole, while the loading applied is not considered. It is also assumed that the pipe would not be jacketed, but is thermally insulated (Antonakas, 1988). The last assumption is that the diameter of the hole remains constant throughout the experiment.

4.2. Experiment Overview

There has been a collaborative effort to design the sodium metal fire experiments that will be conducted at SNL in the near future. Even though the focus of this report was on spray fires, engineers at SNL are also concerned with various other postulated fire scenarios. Their

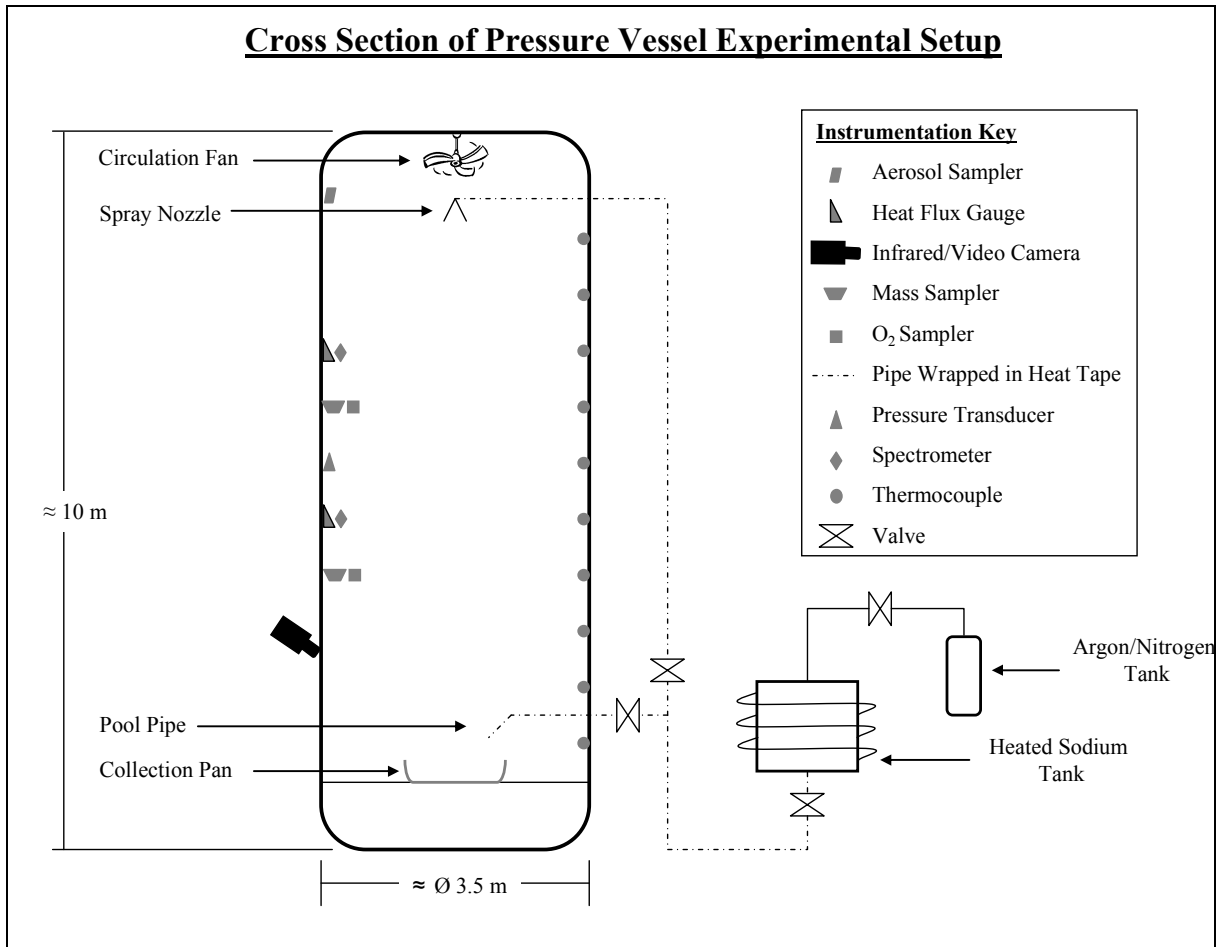
overall goal is to understand the following areas of combustion: radiative feedback from droplets, oxygen penetration into the spray, and the resulting burn rate. The Surtsey pressure vessel, with approximate dimensions of 10 m tall by 3.5 m in diameter, will be used to facilitate these tests. The specifications of the experiment have not yet been decided; however, a general description has been presented below.

Figure 11 shows the Surtsey vessel and Figure 12 shows the proposed experimental setup for the sodium metal fire tests. An argon/nitrogen supply tank may be used to pressurize the sodium holding tank. This holding tank can be heated by the electric coils that surround it. In an effort to keep the sodium at a constant temperature, all of the pipes downstream from the tank will be insulated with heat tape. These heat tape wrapped pipes lead either to the pool pipe or the spray nozzle. The pool pipe will distribute sodium to the collection pan in order to replicate a leak resulting in a pool. The nozzle will be used for the spray fire trials. A combination fire will occur when the sodium that flows out of the spray nozzle does not completely burn before reaching the burn pan, thus resulting in a pool fire. In any situation, the valves can be used to vary the pressures to each of the exits into the vessel. Each of the supply pipes can be isolated using the valves in order to create the different fire scenarios. A circulation fan may be used to mix and unify the environment in the pressure vessel so that measurements will be consistent regardless of the position from which the reading is taken.

Various instrumentation will be used to collect results of the experiment. During the experiments, samples may be extracted from the vessel to analyze aerosol production, mass concentration, and oxygen concentration. The oxygen concentration will be important because it can be the foundation for determining the burning efficiency (i.e. completion of reaction). Also, an infrared/video camera can be used to capture visual results. Pressure transducers and thermocouples can be mounted on the tank to record pressures and temperatures, respectively, at various heights during the testing. A spectrometer and heat flux gauge may also be used to record the intensity of radiation produced by the resulting fire. A data acquisition system will be necessary to record most of the data for the various instruments discussed here. Other specifications and tools may also be selected; however, this general understanding is sufficient for the purposes of this report.



Figure 11: Surtsey Vessel



4.3. Scenario Leak Flow Calculations

Since a sodium leak can occur along a section of piping, it is possible to have a flow in the pipe at stage 1, out of the pipe at stage 2, and through the pipe at stage 3. These flows are depicted in Figure 13. In this situation, the pressure and flow were known values for stage 1, while neither of these values were known for stage 3. However, for the purposes of calculating the velocity out of the pipe using Bernoulli's equation, it was assumed that the pressure and velocity at stage 3 was equal to the values at stage 1. This was assumed because the limitations to the Bernoulli equation of a streamline states the flow conditions in the pipe must not be altered by the flow leaving the pipe. Also, the pressure at stage 2 was defined to be atmospheric, while the velocity was unknown. The velocity at stage 2 was calculated based on these assumptions, given values, and the pressure difference between inside of the pipe (stages 1 and 3) and outside

of the pipe (stage 2). From this velocity, the volumetric and mass flow rates were calculated for various hole diameters.

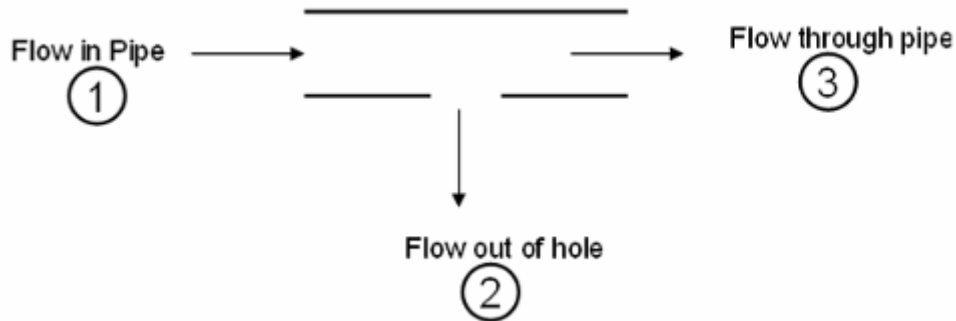


Figure 13: Depiction of Pipe Flow

The pressure differential equation was derived from the energy equation along a streamline, as seen in Equation 4. This equation assumes that the flow was steady, isothermal, and adiabatic.

$$\frac{d}{dt} \int_{V_{os}} \left(\frac{V^2}{2} + gz + u \right) \rho dv + \int_{Ar} \rho \left(h + \frac{V^2}{2} + gz \right) \vec{V} \cdot \vec{n} dA_r = \dot{Q} - \dot{W}$$

Equation 4: Energy Equation along a Streamline
(Alexandrou, 2001)

Since a stationary control volume was of interest, the calculation was independent of time and thus the first term of Equation 4 went to zero. Also, mass flow rate is equal to product of density, velocity, and area, as seen in Equation 5.

$$\dot{m} = \rho VA$$

Equation 5: Mass Flow Rate
(Alexandrou, 2001)

The streamline was formed by one point in the pipe flow and a second arbitrary point outside of the pipe, which allows the energy equation to be shortened to Equation 6. Either the values for stage 1 or stage 3 could have been used for the calculations because they were assumed to be equal, as explained above.

$$\dot{m} \left[(h_2 - h_1) + \left(\frac{V_2^2}{2} - \frac{V_1^2}{2} \right) + g(z_2 - z_1) \right] = 0$$

**Equation 6: Shortened Energy Equation
(Alexandrou, 2001)**

Since enthalpy is equal to the internal energy plus the pressure divided by the density, as seen in Equation 7, and because the flow was assumed to be isothermal, the equation was rewritten as seen in Equation 8.

$$h = u + \frac{P}{\rho}$$

**Equation 7: Enthalpy Equation
(Alexandrou, 2001, 95)**

$$\left(\frac{P}{\rho} + gz + \frac{V^2}{2} \right)_1 = \left(\frac{P}{\rho} + gz + \frac{V^2}{2} \right)_2 = \text{const.}$$

**Equation 8: Bernoulli Equation
(Alexandrou, 2001)**

With the assumptions stated above, the Bernoulli equation was rearranged into Equation 9, where V_{out} = velocity out hole, C_D = discharge coefficient, P_{in} = pressure in pipe, and P_{out} = pressure outside pipe. Calvert defines the coefficient of discharge as equal to the product of the coefficient of contraction and the coefficient of velocity. The coefficient of contraction is equivalent to the difference of the jet and hole area. For an ideal hole, as is assumed in this case, the coefficient of contraction is 0.62. The coefficient of velocity is usually quite high, between 0.95 and 0.99 (Calvert, 2003). In this situation, it was assumed to be 0.98, therefore, the coefficient of discharge was calculated to be 0.61.

$$V_{out} = C_D \sqrt{\frac{2(P_{in} - P_{out})}{\rho}}$$

**Equation 9: Leak Spray Exit Velocity Equation
(Alexandrou, 2001)**

From the velocity calculated in Equation 9, it was possible to calculate the volumetric and mass flow rates by using Equation 5 and Equation 10, where ρ = fluid density, A = cross-sectional area of pipe, and V = pipe flow velocity.

$$Q = VA$$

**Equation 10: Volumetric Flow Rate
(Alexandrou, 2001)**

Engineers from SNL postulated three scenarios in which a potential sodium leak could occur. The constants of each scenario can be seen in Table 3. Based on these constants, the velocity out of the hole was calculated for each scenario and shown in Table 4. These leak velocities were then used to calculate the volumetric and mass flow rates for various sized holes in each scenario. These results are shown in Table 5, as well as Figure 14, Figure 15, and Figure 16.

	Scenario A	Scenario B	Scenario C
Density (kg/m ³)	830	870	870
Temperature (°C)	488	326	333
Absolute Pressure Inside Pipe (kPa)	200	300	120
Absolute Pressure Outside Pipe (kPa)	101	101	101
Pipe Mass Flow Rate (kg/s)	628	645	21.5
Pipe Flow Velocity (m/s)	5.2	6.5	0.2
Pipe Outside Diameter (m)	0.4	0.4	0.4
Pipe Wall Thickness (m)	0.01	0.01	0.01
Pipe Inside Diameter (m)	0.38	0.38	0.38
Pipe Flow Rate (gpm)	9380	11700	390
Discharge Coefficient	0.61	0.61	0.61

Table 3: Scenario Constants

	Scenario A	Scenario B	Scenario C
Leak Velocity (m/s)	9.5	13	4.1

Table 4: Velocity out of Hole Results

Hole Diameter (mm)	Volumetric Flow Rate (gpm)			Mass Flow Rate (kg/s)		
	Scenario A	Scenario B	Scenario C	Scenario A	Scenario B	Scenario C
1	0.1	0.2	0.1	0.01	0.01	0.003
2	0.5	0.7	0.2	0.02	0.04	0.01
3	1.1	1.5	0.5	0.1	0.1	0.03
4	1.9	2.6	0.8	0.1	0.1	0.05
5	3.0	4.1	1.3	0.2	0.2	0.1
6	4.3	5.9	1.9	0.2	0.3	0.1
7	5.8	8.0	2.5	0.3	0.4	0.1
8	7.6	10	3.3	0.4	0.6	0.2
9	9.6	13	4.2	0.5	0.7	0.2
10	12	16	5.1	0.6	0.9	0.3
20	47	65	21	2.5	3.6	1.1
30	107	146	46	5.6	8.1	2.5
40	190	260	82	10	14	5
50	296	407	129	16	22	7
60	427	586	185	22	32	10

Table 5: Flow Rate Results

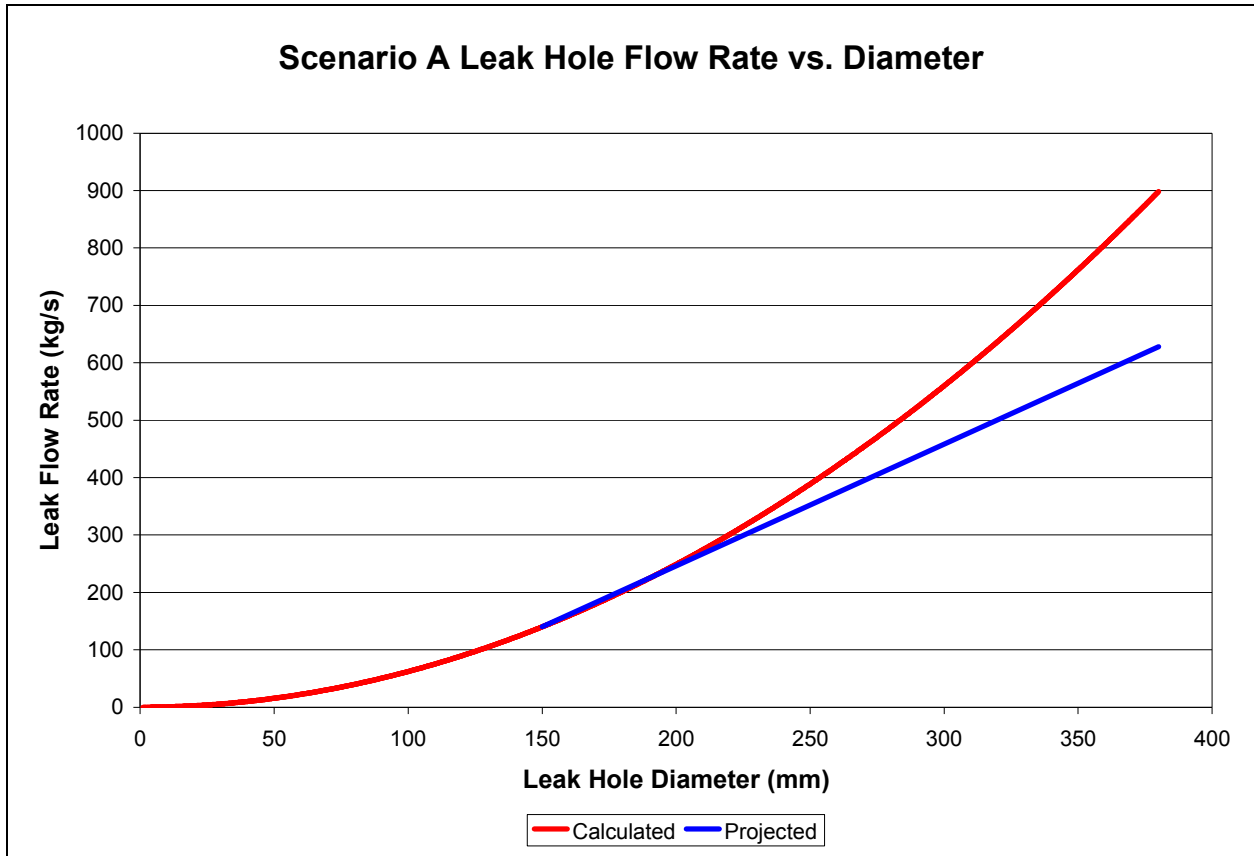


Figure 14: Scenario A Leak Flow Rate

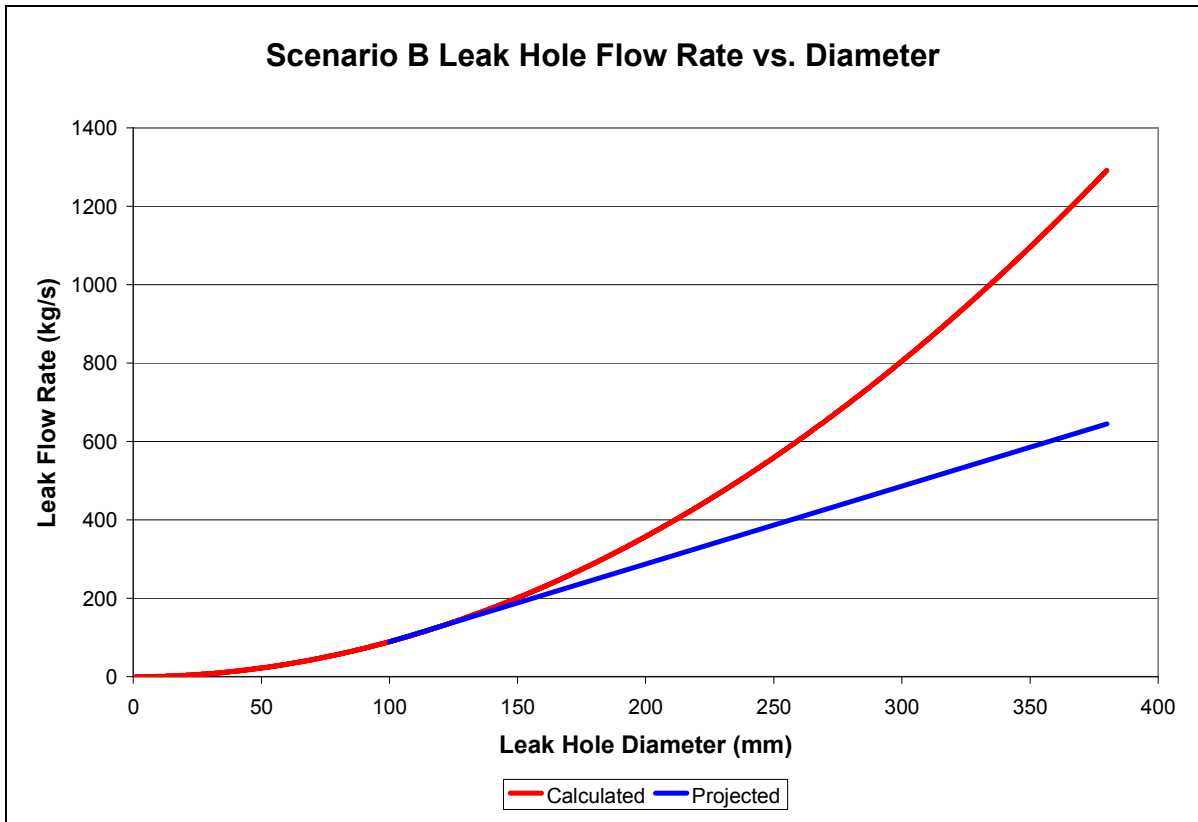


Figure 15: Scenario B Leak Flow Rate

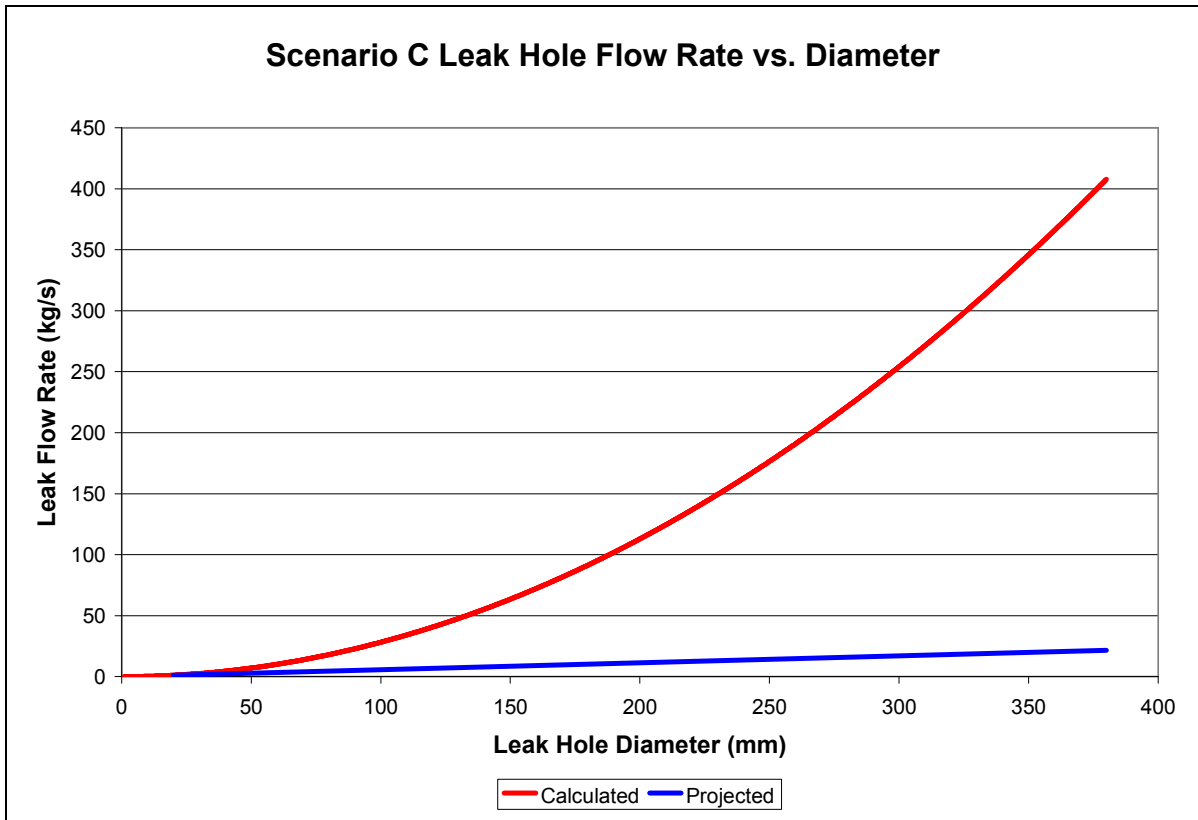


Figure 16: Scenario C Leak Flow Rate

There are limitations to the technique used here, such as the exit velocity and flow predictions are only valid up until a certain leak hole diameter. This is because there is a point at which the hole will become large enough to cause the pressure inside the pipe to change, thus changing the flow conditions and invalidating Bernoulli's equation. As a result, the calculated velocity and flow rates will be incorrect for flows out of a hole that are larger than the limiting hole size. In Figure 14, Figure 15, and Figure 16 the red curve shows the estimated calculation of flow rate out of the leak using the method described in Equation 4 through Equation 10, while the blue line represents the forecasted leak flow rate. The forecasted leak flow rate was determined by assuming the maximum leak flow out of the pipe would occur if a guillotine cut of the pipe was made. It was assumed that in this case the maximum leak flow could be no greater than the flow assumed in the pipe. However, if a full pipe rupture were to occur then the actual flow rate out the end of the pipe would be greater than this maximum flow rate. On the chart, from the point of the assumed maximum leak flow, a linear transition was made to a point on the red calculated curve in which the blue line was tangent. The intersection point was said to be the upper leak hole limitation of the Bernoulli equation. As a result, the leak flow rate can be estimated by using the Bernoulli calculation method for holes up to the limitation and by use of the forecasted method for holes larger than the intersection point. For Scenarios A, B, and C the values of this limitation point are 0.15 m, 0.1 m, and 0.02 m, respectively. The use of these methods will not be exact, but will be a good approximation of the leak flow rate for various size holes.

4.3.1. Sodium Flow from a Nozzle as Compared to Water

Each nozzle provided by Spraco, Inc. is characterized by the flow rate of the liquid exiting the nozzle and the pressure in the nozzle. Because the flow rate for each nozzle is given in terms of water, the corresponding flow rate of sodium must be calculated in order to compare this against the calculated leak flow rates for the postulated scenarios. Thus, the specific gravity, SG, must first be calculated. The specific gravity is a dimensionless value defined as the ratio of the density of a material and the density of water (Spraco, Inc., 1983). This equation is shown in Equation 11, where ρ_s = density of liquid sodium and ρ_w = density of liquid water.

$$SG = \frac{\rho_s}{\rho_w}$$

**Equation 11: Specific Gravity
(Spraco, Inc., 1983)**

The *Spray Nozzle User's Manual* describes that “the flow rate varies inversely as the square root of the specific gravity of a liquid (neglecting the effect of all other factors)” (Spraco, Inc., 1983). Based on this information, the manual also provides conversion factors for specific gravities ranging from 0.7 to 1.8 that can be used to convert the flow rate of water out of a nozzle to the flow rate of a desired liquid. The equation to complete this conversion is seen in Equation 12, where Q_s = flow rate of desired liquid (sodium), Q_w = flow rate of water, and CF = conversion factor (Spraco, Inc., 1983). Because the flow rate of sodium was calculated in section 4.2, these flow rates were converted to the equivalent flow rate of water.

$$\dot{Q}_s = \dot{Q}_w \times CF$$

**Equation 12: Flow Rate Conversion
(Spraco, Inc., 1983)**

The input values and results of the specific gravity calculations, as well as the resulting values of the conversion factors, are shown in Table 6. The results of the flow conversion calculations are shown in Table 7. Because the values of the density of sodium are close to that of water, the conversion factor of scenario A is 1.12, and 1.05 for scenarios B and C (Spraco, Inc., 1983). These values of the conversion factor resulted in a very small change in the flow rate out of the nozzle of water as compared to sodium. These converted flow rates of water will be used in choosing specific nozzles for the experiments, as seen in Section 4.6.

	Scenario A	Scenario B	Scenario C
Density of Water (kg/m ³)	997	997	997
Density of Sodium (kg/m ³)	830	870	870
Specific Gravity of Sodium	0.8	0.9	0.9
Conversion Factor	1.12	1.05	1.05

Table 6: Densities, Specific Gravity, and Conversion Factors

Diameter of Hole (mm)	Scenario A		Scenario B		Scenario C	
	Sodium	Water	Sodium	Water	Sodium	Water
1	0.01	0.01	0.01	0.01	0.003	0.003
5	0.2	0.1	0.2	0.2	0.1	0.1
10	0.6	0.6	0.9	0.9	0.3	0.3
20	2.5	2.2	3.6	3.4	1.1	1.1
30	5.6	5.0	8.1	7.7	2.5	2.4
40	10	8.9	14	14	4.5	4.3
50	16	14	22	21	7.1	6.7
60	22	20	32	31	10	9.7

Table 7: Flow Rate Conversion Results

4.3.2. Sodium Droplet Diameter as Compared to Water

Fluid properties differ between sodium and water, therefore the diameter of the droplets that are produced when the liquid flows from a nozzle will also be different. The two most important properties are density and surface tension, which can be found in Table 8.

	Density @ 100 °C	Surface Tension
Sodium	$\rho_{sodium} = 927 \frac{kg}{m^3}$	$\sigma_{sodium} = 0.19 \frac{N}{m}$
Water	$\rho_{water} = 958 \frac{kg}{m^3}$	$\sigma_{water} = 0.072 \frac{N}{m}$

Table 8: Properties of Sodium and Water
(Incropera and DeWit, 2002)

A simple method to determine the difference in droplet diameters is to consider a moving cylindrical control volume, shown in Figure 17. A surface tension force, Equation 13, acts in the opposite direction of motion while an inertial force, Equation 14, acts in the direction of motion. The point at which these forces are balanced is when droplets start to shed. Nomenclature for the surface tension force and inertial force σ equations is: R = Radius of cylinder, σ = Surface tension, V = Velocity, ρ = Density, and L = Characteristic length (Cross-sectional area).

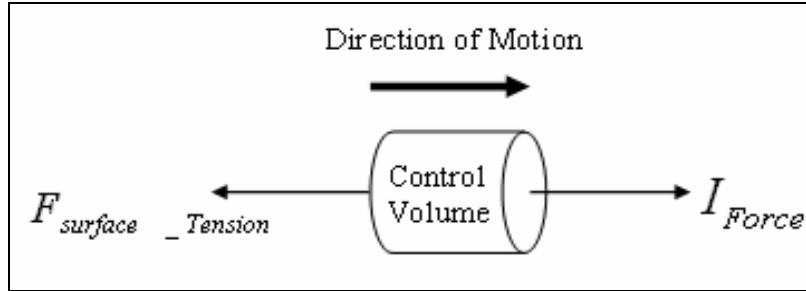


Figure 17: Spray Droplet Control Volume

$$F_{surface_Tension} = 2\pi R * \sigma$$

Equation 13: Surface Tension Force
(Alexandrou, 2001)

$$I_{Force} = \rho V^2 A$$

Equation 14: Inertial Force
(Alexandrou, 2001)

Equation 13 and Equation 14 are set equal to each other in Equation 15, which represents the point at which the droplets will start to shed.

$$2\pi R * \sigma = \rho V^2 A$$

Equation 15: Balance of Forces

The balance of forces can be rearranged and solved for the droplet radius, as shown in Equation 17. Two different calculations have been completed, one with the properties and velocity of water and the other with the properties and velocity of sodium. The velocities of the two fluids were calculated by using the method described in sections 4.3 and 4.3.1. First the flow rates were calculated, then the velocities were determined from Equation 16, where Q = volumetric flow rate and A = cross-sectional area. 508-334-9900 option 2

$$V = \frac{Q}{A}$$

Equation 16: Velocity from Volumetric Flow Rate
(Alexandrou, 2001)

$$R = \frac{2\sigma}{\rho V^2}$$

Equation 17: Radius of Droplet Calculation

The ratio of the droplet diameters for sodium and water can be found using Equation 18, in order to determine how much larger the sodium droplet will be as compared to the water droplet.

$$Ratio = \frac{R_{Sodium}}{R_{Water}}$$

Equation 18: Ratio of Droplet Radii

Using this method, it was determined that the diameter of the sodium droplet will be about 2.2 times larger than the diameter of the water droplet. Details can be seen in Appendix A.

4.4. Spray Formation

The transformation of a liquid jet into droplets as it enters another fluid, thus creating a spray, has been greatly studied in an attempt to understand the mechanisms of breakup. The beginning stages of spray formation are determined by unstable movements in the jet, while the later stages of spray formation are thought to be chaotic (Mitra and Li, n.d.). The most frequently studied liquid jet is one that is injected through a circular hole into a stagnant gas. These studies have shown that the resulting spray is affected by the exit velocity of the jet, the profile and turbulence at the nozzle exit, the internal flow effects of the nozzle, and the physical/thermodynamic states of the liquid/gas (Lin and Reitz, 1998).

There are many theories and studies which explore the cause of breakup in a liquid jet. Lin and Reitz found that a disturbance beginning at the nozzle tip grows in space as it travels downstream and breaks the jet into droplets while leaving a length of jet unbroken near the nozzle tip. While all jets are broken up due to these disturbances, the exact breakup can differ. Four distinct breakup regimes have been identified: the Rayleigh regime, the first wind-induced regime, the second wind-induced regime, and the atomization regime. Each of the four regimes

can be seen in Figure 18 in the same order as listed above, where “a” is the Rayleigh regime and “d” is the atomization regime (Lin and Reitz, 1998).

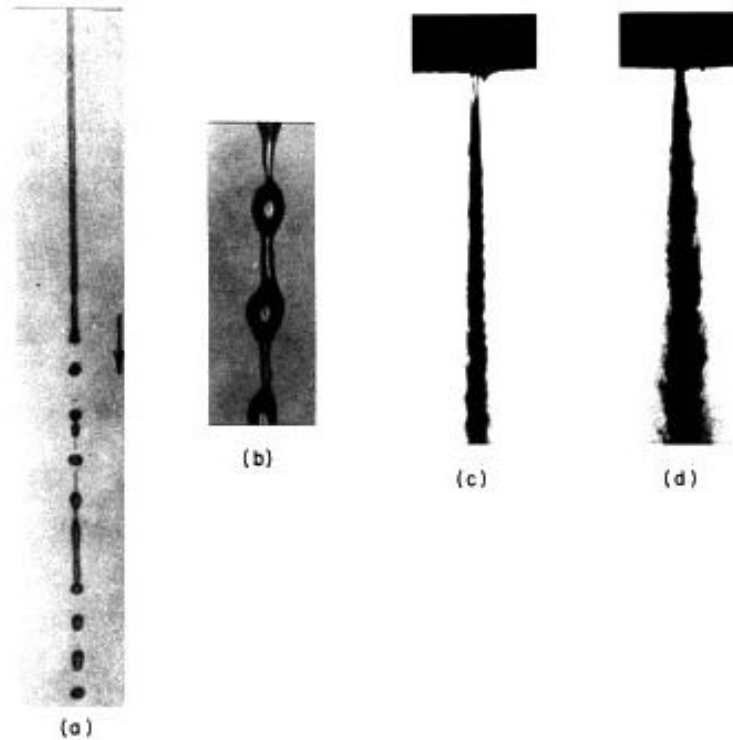


**Figure 18: Breakup Regimes
(Lin and Reitz, 1998)**

Lin and Reitz describe that the Rayleigh and first wind-induced regimes occur when a liquid is injected through a nozzle at low velocities. Disturbances in the jet create droplets with diameters equal to or larger than the diameter of the jet (Lin and Reitz, 1998). As can be seen in Figure 18a, the Rayleigh regime is characterized by a relatively long, unbroken jet before droplets of a larger diameter than the jet break off. Figure 18b shows that the first wind-induced regime is also characterized by droplets of diameters larger than the jet. However, these droplets are connected by sections of unbroken jet, rather than breaking off completely.

At high jet velocities the second wind-induced and atomization regimes occur. Lin and Reitz describe that disturbances break up the jet into droplets with much smaller diameters than the jet. Figure 18 shows that because jets in both the second wind-induced and atomization regimes are the droplets small diameters create a fine spray for each regime. For the second

wind-induced regime this breakup begins to occur some distance away from the nozzle, while for the atomization regime the fine spray begins to develop at the nozzle. Because of the fine spray that surrounds the jet in these regimes, it is difficult to view the details of the jet near the nozzle. The fine spray also makes it difficult to see the surface waves which cause the disturbance and breakup (Lin and Reitz, 1998).

As described earlier, the jets in each regime break up due to disturbances along the jet. These disturbances, along with the liquid inertia and surface tension, determine which regime will result for a particular jet. However, the exact mechanism of breakup is not fully understood. This is particularly true for the atomization regime, although many theories have been proposed. Reitz and Bracco have explored these theories and found that not one of them alone is able to predict results consistent with those collected in experiments. However, it is thought that a combination of theories, as well as taking into account the nozzle geometry, may be able to accurately match experimental results. Because the effects of the nozzle geometry are unknown, it may not be possible to test this theory or develop it further at this time (Reitz and Bracco, 1982).

Since the combination of liquid inertia, surface tension, and aerodynamic forces acting on the jet determine which breakup regime will occur, Lin and Reitz have used the Weber number to quantify the four regimes. The Weber number is a dimensionless value defined as the ratio of the inertia force to the surface tension force acting on the jet. The end of the Rayleigh regime is said to be when dripping no longer occurs at the nozzle exit or when the Weber number of the gas is less than 0.4. For this value, the gas reaches approximately 10% of the surface tension force and therefore its effects must be accounted. The second wind-induced regime begins when the Weber number of gas is greater than 13; this is when the effects of the ambient gas become dominant to the surface tension force. The atomization regime begins when the Weber number is greater than 40.3 (Lin and Reitz, 1998).

Equation 19 is used to calculate the Weber number of air, where We_g = Weber number of air, ρ_2 = density of air at standard ambient temperature, U = jet exit velocity, a = jet radius, and σ = surface tension of sodium (Lin and Reitz, 1998).

$$We_g = \frac{\rho_2 U^2 (2a)}{\sigma}$$

**Equation 19: Weber Number of Air
(Lin and Reitz, 1998)**

The density of air and the surface tension of sodium are known values (Incropera and DeWit, 2002), while the jet exit velocity was calculated in section 4.2. The values used in the calculations are shown in Table 9.

Density of Air (kg/m ³)	1.17
Surface Tension of Liquid Sodium (N/m)	0.19
Jet Exit Velocity - Scenario A (m/s)	9.5
Jet Exit Velocity - Scenario B (m/s)	13
Jet Exit Velocity - Scenario C (m/s)	4.1

Table 9: Input Values for Weber Equation

The radius of the jet was calculated by completing Equation 20 and Equation 21, where A = area of jet, A_0 = area of hole, and C_c = coefficient of contraction (Calvert, 2003). The results of these calculations differ based on the hole diameter chosen and can be seen in Table 10.

$$A = A_0 C_c$$

**Equation 20: Area of Jet
(Calvert, 2003)**

$$a = \sqrt{\frac{A}{\pi}}$$

**Equation 21: Radius of Jet
(Calvert, 2003)**

Diameter of Hole (mm)	10	20	30	40	50	60
Area of Hole (mm ²)	79	314	707	1257	1963	2827
Coefficient of Contraction	0.62	0.62	0.62	0.62	0.62	0.62
Area of Jet (mm ²)	49	195	438	779	1217	1753
Radius of Jet (mm)	3.9	7.9	12	16	20	24

Table 10: Results of Jet Radius Calculations

Based on the given and calculated values, the Weber number of air was calculated for the various hole diameters, these results are shown in Table 11. The table also shows the formation regime which corresponds to the Weber number calculated for each hole diameter and scenario.

Hole Diameter (mm)	Scenario A		Scenario B		Scenario C	
	Weber Number	Breakup Regime	Weber Number	Breakup Regime	Weber Number	Breakup Regime
10	4.4	1st wind-ind.	8.3	1st wind-ind.	0.8	1st wind-ind.
20	8.7	1st wind-ind.	17	2nd wind-ind.	1.6	1st wind-ind.
30	13	2nd wind-ind.	25	2nd wind-ind.	2.4	1st wind-ind.
40	17	2nd wind-ind.	33	2nd wind-ind.	3.3	1st wind-ind.
50	22	2nd wind-ind.	42	Atomization	4.1	1st wind-ind.
60	26	2nd wind-ind.	50	Atomization	4.9	1st wind-ind.

Table 11: Weber Number Results

For each of these regimes, the internal effects of the nozzle are not considered within the Weber number calculations. While it is possible to calculate initial disturbance effects of the nozzle internal flow phenomena for jets in the atomization regime based on calculations presented in Lin and Reitz (1998), it is not necessary in order to show the flow formation in a postulated leak scenario. In the case of a hole, it is assumed that there are no internal effects as would be seen with a nozzle. Thus, the calculated Weber numbers and corresponding regimes are assumed to be correct.

4.5. Necessary Nozzle Height for Complete Burning

An experimental specification for the spray fire tests is for the sodium to completely burn before reaching the spill pan. In order to accomplish this, the distance above the spill pan at which the sodium will be sprayed must be calculated. A burn rate for a single falling droplet subjected to forced convection, which was experimentally determined to be 170 mg/s, was assumed for these height calculations since it closely represents the situation that will be carried out in these experiments (Rockwell International, 1975). The assumptions and conditions associated with this burn rate can be found in Section 3.2.1. It was also assumed that the droplets are perfect spheres and remain at a constant density.

For a particular droplet diameter, the volume of the sphere can be calculated from Equation 22, where V = volume of droplet and r = radius of droplet.

$$V_{sphere} = \frac{4}{3} \pi r^3$$

Equation 22: Volume of a sphere

From here, the volume could be converted into a mass of sodium with the use of density, as seen in Equation 23, where ρ = density of sodium, m = mass of sodium, and V = volume of droplet. Properties of sodium can be found in Section 2.3.1.

$$m = \rho V$$

Equation 23: Density Equation

Next, the time needed for the droplet to completely burn ($t_{complete_burn}$) was calculated. This was done by dividing the mass (m) of the droplet by the assumed mass burning rate (Br), as seen in Equation 24.

$$t_{complete_burn} = \frac{m}{Br}$$

Equation 24: Time for Complete Droplet Burning

This time is then used to calculate the necessary distance in order for complete burning of the droplet to occur, as seen in Equation 25, where ΔY = necessary falling distance, v_{y0} = initial velocity, t = time for complete burn, and a_y = acceleration (gravity).

$$\Delta Y = v_{y0} t + \frac{1}{2} a_y t^2$$

**Equation 25: Falling Distance for Complete Burn
(Serway and Beichner., 2000)**

For the three scenarios described in Section 4.3, Table 13, Table 14, and Table 15 show the distances (i.e. Required Height) needed for complete burning of various diameter droplets,

while Table 12 shows the specifications for the scenarios. The distances needed for complete burning of various diameter droplets at 450 °C and 500 °C that are injected at various velocities can be found in Table 16 or Appendix B. Figure 19 graphically compares the required height for complete burning versus the droplet diameter for the various situations. Figure 20 graphically compares the required height for complete burning versus various velocities for a 4 mm droplet.

	Scenario A	Scenario B	Scenario C
Sodium Density (kg/m ³)	830	870	870
Initial Velocity (m/s)	9.5	13	4.1

Table 12: Required Height Scenario Specifications

Droplet Diameter (mm)	Droplet Volume (m ³)	Mass (mg)	Time to Full Burn (sec)	Required Height for Complete Burn (m)
1	5.2E-10	0.4	0.003	0.02
2	4.2E-09	3.5	0.02	0.2
3	1.4E-08	12	0.1	0.7
4	3.4E-08	28	0.2	1.7
5	6.5E-08	54	0.3	3.6
6	1.1E-07	94	0.6	6.8
7	1.8E-07	149	0.9	12
8	2.7E-07	223	1.3	21
9	3.8E-07	317	1.9	35
10	5.2E-07	435	2.6	57

Table 13: Scenario A Required Height

Droplet Diameter (mm)	Droplet Volume (m ³)	Mass (mg)	Time to Full Burn (sec)	Required Height for Complete Burn (m)
1	5.2E-10	0.5	0.003	0.04
2	4.2E-09	3.6	0.02	0.3
3	1.4E-08	12	0.1	1.0
4	3.4E-08	29	0.2	2.4
5	6.5E-08	57	0.3	4.9
6	1.1E-07	99	0.6	9.2
7	1.8E-07	156	0.9	16
8	2.7E-07	234	1.4	27
9	3.8E-07	333	2.0	44
10	5.2E-07	456	2.7	70

Table 14: Scenario B Required Height

Droplet Diameter (mm)	Droplet Volume (m ³)	Mass (mg)	Time to Full Burn (sec)	Required Height for Complete Burn (m)
1	5.2E-10	0.5	0.003	0.01
2	4.2E-09	3.6	0.02	0.1
3	1.4E-08	12	0.1	0.3
4	3.4E-08	29	0.2	0.9
5	6.5E-08	57	0.3	1.9
6	1.1E-07	98	0.6	4.0
7	1.8E-07	156	0.9	7.9
8	2.7E-07	233	1.4	15
9	3.8E-07	332	2.0	27
10	5.2E-07	455	2.7	46

Table 15: Scenario C Required Height

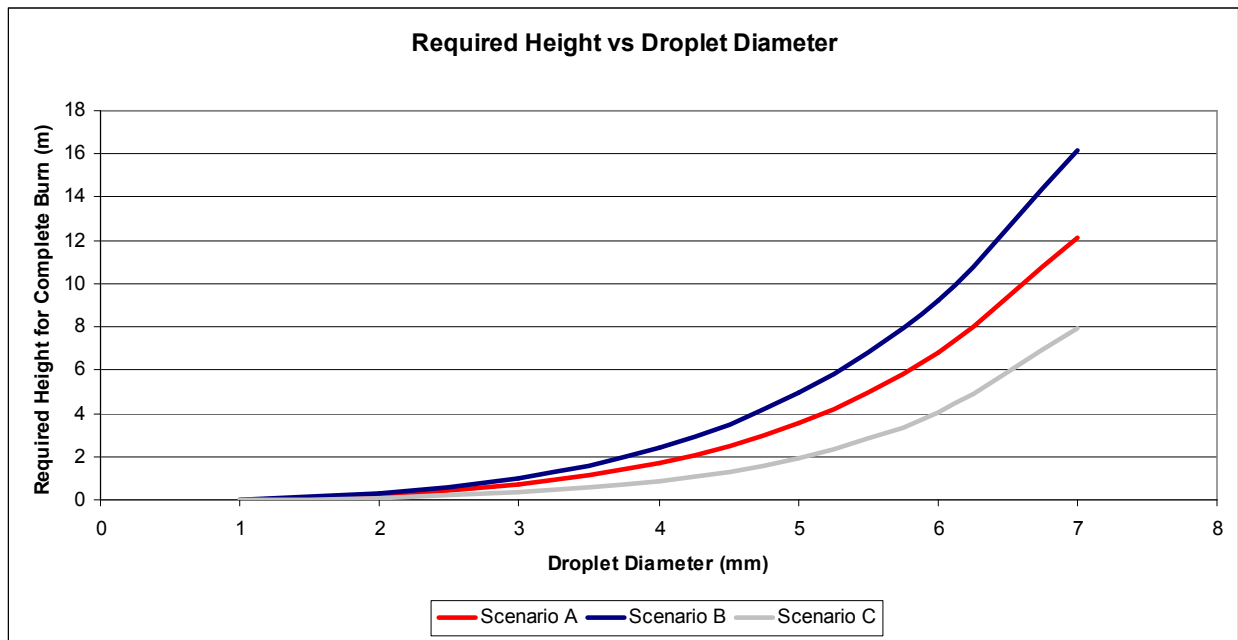


Figure 19: Three Scenarios Required Height

Droplet Diameter (mm)	Required Height for Complete Burn (m)				
	V = 1 m/s	V = 5 m/s	V = 11 m/s	V = 17 m/s	V = 20 m/s
1	0.003	0.01	0.03	0.04	0.05
2	0.02	0.1	0.2	0.3	0.4
3	0.1	0.4	0.8	1.2	1.4
4	0.3	0.9	1.9	2.9	3.4
5	0.8	2.1	4.0	5.9	6.9
6	2.0	4.2	7.6	11	13
7	4.6	8.1	13	19	21

Table 16: 500 °C Sodium Required Height at various Velocities

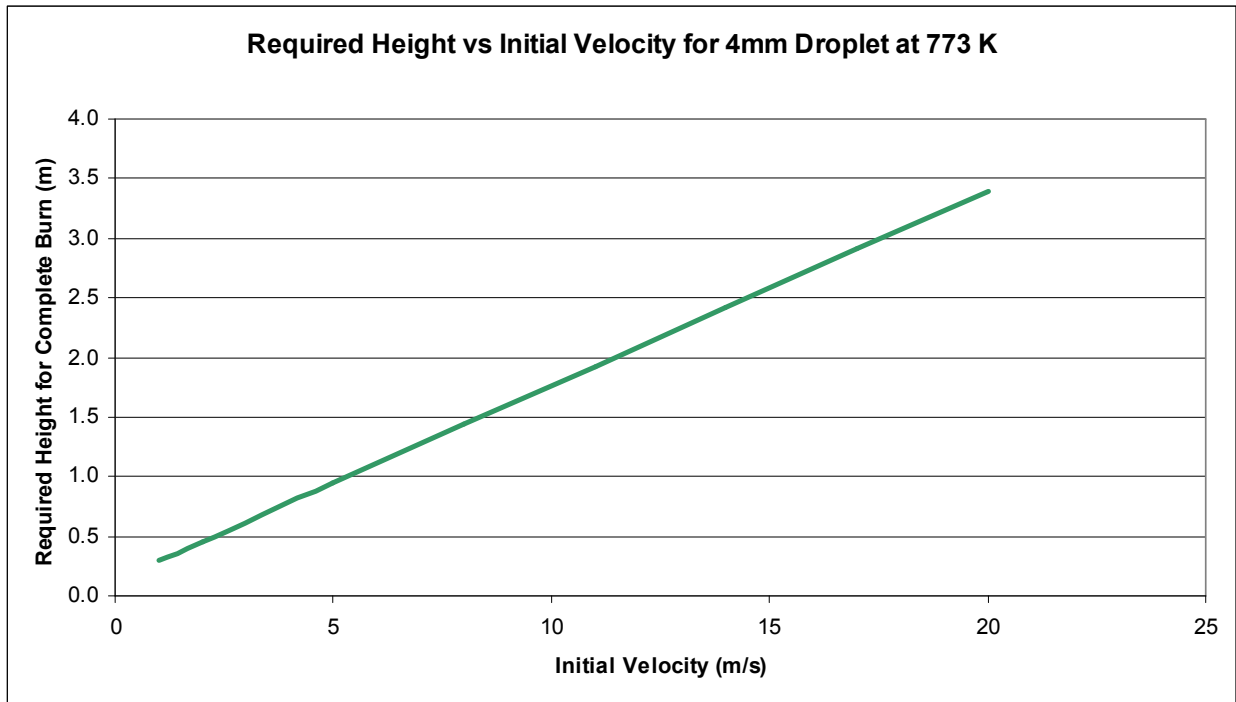


Figure 20: 500 °C Sodium Required Height at various Velocities

The heights shown in the tables above are estimates which incorporate many basic assumptions. The burn rate used for the calculations only accounts for single droplets, not sprays, and thus, not the heat transfer between droplets. For the purposes of these experiments, the heights are good approximations for preliminary experimental design.

4.6. Nozzle Selection

The goal of the experiments is to gather data of spray fires that will result in a more advanced understanding of sodium spray combustion phenomena. As can be seen in section 4.4, all but two of the postulated leak scenarios form jets in the first wind-induced or second wind-induced regimes. While these regimes technically produce sprays, in order to understand the fundamentals of spray combustion, a spray with a finer droplet pattern is needed. For this reason, spray nozzles will be used. The nozzles will be operated within the range of the postulated leak hole's diameter, pressures, and flow rates; however, they may not exactly simulate each leak.

While there are numerous specialty nozzles available for manufacturing, there are four basic categories of nozzles available from various manufacturers, such as Spraco, Inc.: the flat fan nozzle, the full cone nozzle, the hollow cone nozzle, and the atomization nozzle. Each of these categories contains numerous nozzle designs that differ in internal design, spray angle, operating pressures, operating flow rates, droplet diameter, and droplet distribution (Spraco, Inc., 1983). In order to choose an effective nozzle for the experiments, it is important to understand the advantages and disadvantages of each category.

The flat fan nozzle is depicted in Figure 21 and produces a spray of fluid into a thin line which grows in length as the fluid increases its distance away from the nozzle. Flat fan sprays are most often used for cleaning or washing applications when a high impact spray is desired. It is explain that minimizing the height of the nozzle from the target and narrowing the spray angle will increase the impact (TPS, Inc., 2001). It is also described that “the impact received is directly related to the density of the spray pattern, so the tighter you maintain the spray pattern, the more impact per in² will be received” (TPS, Inc., 2001). Since the spray is contained to one thin line, it appears that oxygen could be evenly and easily transported to each droplet, thus increasing the burn rate of the spray.

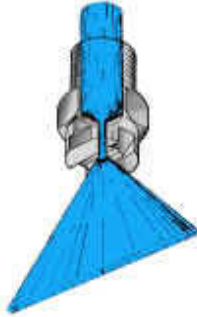


Figure 21: Flat Fan Nozzle and Spray
(TPS, Inc., 1999)

The full cone nozzle, shown in Figure 22, is also used in cleaning and washing applications that require uniform distribution over a full cone area (Lechler, 1992). TPS, Inc. shows how the fluid exits the nozzle in a solid cone pattern made up of droplets with diameters that are considered to be fine to coarse. While full cone nozzles are used for similar applications as the flat fan nozzle, the impact of the spray originating from a full cone nozzle is not as great. As with the flat fan nozzle, the impact of the full cone nozzle can be increased by narrowing the spray angle and decreasing the nozzle height from the target (TPS, Inc., 2001).

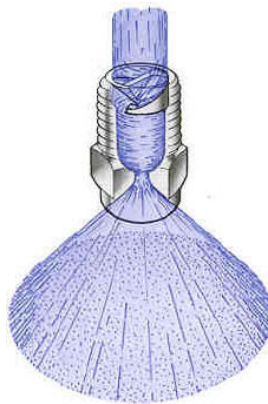


Figure 22: Full Cone Nozzle and Spray
(TPS, Inc., 1999)

While the hollow cone nozzle, shown in Figure 23, produces a spray with a cone pattern similar to that of a full cone nozzle, the hollow cone nozzle creates a “ring-shaped impact area” (Lechler, 1992). TPS, Inc. explains how this type of nozzle breaks up the spray into fine droplets that have diameters ranging from 0.004 cm to 0.05 cm. These fine droplets make this nozzle ideal for gas conditioning applications, such as evaporative cooling (TPS, Inc., 2001). Since a

decrease in droplet diameter increases the burn rate, it can be assumed that the burn rate of a spray from a hollow cone nozzle will be greater than that from a full cone nozzle (Krolikowski, 1968).



Figure 23: Hollow Cone Nozzle and Spray
(TPS, Inc., 1999)

For both the full and hollow cone nozzles, TPS, inc. provides a nozzle that is designed with or without internal vanes. An example of a vaneless hollow cone nozzle can be seen in Figure 24. While each variation of the nozzles creates the same spray pattern (either full or hollow cone), nozzles without vanes reduce clogging of the nozzle. Clogging is reduced because the largest particle that can pass through the nozzle is increased in comparison to the largest particle that can pass through an internal vane. This comparison is only relevant for nozzles whose only difference is the presence or absence of internal vanes (TPS, Inc., 2001).

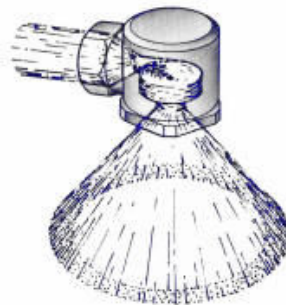


Figure 24: Vaneless Hollow Cone Nozzle and Spray
(TPS, Inc., 1999)

TPS, Inc. describes three possible atomization nozzles: twin fluid, hydraulic, and ultrasonic. A twin fluid atomization nozzle can be seen in Figure 25. Atomization nozzles create

sprays that are fine to very fine, with diameters as small as 0.001 cm, and thus are used in cooling and gas conditioning applications as with the hollow cone nozzle. Atomizing nozzles are also used in applications of lubricating, coating, and moisturizing. Twin fluid atomizing nozzles, which use air to atomize the liquid, create either a full or flat cone patterned spray (TPS, Inc., 2001). This increases the advantages of these types of nozzles because the same pattern is created from much smaller droplets. However, atomization nozzles have the disadvantage for this experiment of operating with much lower flow rates than the other nozzles discussed. While TPS, Inc. shows that the flat fan, full cone, and hollow cone nozzles have flow rates that are measured in gpm, the flow rate of the atomization nozzles are measured in gallons per hour (TPS, Inc., 2001). Based on the flow rates for the postulated leaks in Scenarios A, B, and C, which are measured in gpm, it may not be possible to find an atomization nozzle which operates at a large enough flow rate.



**Figure 25: Twin Fluid Atomization Nozzle with Flat Fan Spray Pattern
(TPS, Inc., 1999)**

The most important piece of information about a nozzle for this experiment is the size of the droplets produced. It is very important that the nozzle chosen does not create droplets which are too large and will not completely burn before reaching the bottom of the experiment vessel. As can be seen in Section 4.5, in each of the three scenarios, sodium droplets must be 6 mm (6000 μm) or smaller in diameter in order to completely burn in the approximate 10 m distance available within the Surtsey vessel. Using the scaling factor calculated in Section 4.3.2, a water droplet must be 2.8 mm (2800 μm) or smaller in diameter. In order to observe the most burning time as possible, it is desirable for the diameter of the sodium droplets to be as close to this limit

as possible. Table 1, which displays information provided by TSP, Inc. for water droplet, shows the approximate droplet diameters that can be expected by each category of spray nozzles. It is clear that the droplets produced by an atomization would be too small. While a hollow cone nozzle can produce droplets with diameters for water between 40 μm and 500 μm (TPS, Inc., 2001), this range is still too small for the purposes of this experiment. Since both the flat fan and hollow cone nozzles are described as creating fine droplets, it has been assumed that the flat fan droplet diameters will be approximately equal to that of the hollow cone nozzle. This concludes that the full cone nozzle, which produces droplets with diameters of approximately 500 μm or greater for water, is the appropriate choice for these experiments.

Nozzle Category	Droplet Description	Approximate Droplet Diameter of Water (m)
Flat Fan	fine	40 μm to 500 μm (assumed)
Full Cone	fine to coarse	> 500 μm
Hollow Cone	fine	40 μm to 500 μm
Atomization	fine to very fine	10 μm to 40 μm

**Table 17: Droplet Description and Diameters
(TPS, Inc., 2001)**

While manufactures of spray nozzles, such as Lechler, do provide the pressures and flow rates for each nozzle model, they do not provide the droplet diameters produced by each nozzle model in their catalogs (Lechler, 1992). Because of this, it is not possible to be positive that the droplets produced will be within the correct diameter range. However, Blanchat *et al.* has completed a series of tests on full cone nozzles that, in part, characterized the droplet diameter of water for a series of pressures and flow rates. These tests showed that for a pressures ranging from 100 to 1400 kPa, the mean droplet diameters ranged from 303.5 μm to 1155.1 μm . This supports the idea that full cone nozzle will produce droplets with diameters approximately equal to and larger than that of a hollow cone nozzle. It also supports the idea that droplets produced by a full cone nozzle would not exceed the 2.8 mm (2800 μm) limit for a water droplet.

Based on the choice of a full cone nozzle, Lechler’s catalog has been reviewed to identify the group of nozzles which most closely match the exit diameters, pressures, and flow rates postulated for scenarios A, B, and C. It can be seen that the Axial Full Cone Large Capacity Nozzles offer various models which closely match the values of the postulated scenarios, as well

as other a broader range of values that may be explored during the experiments. Appendix C shows the comparison of specific nozzle models with scenario specifications for multiple hole diameters. From these tables, it can be seen that Lechler nozzles 461.124, 461.364, 403.524, and 403.624 can simulate all three of the postulated scenarios (Lechler, 1992).

4.7. Measurement Techniques

Past theoretical and experimental work has been reviewed in Section 3.2 to understand the combustion of sodium. From this work it is clear that droplet diameter and oxygen concentration affect the combustion of sodium sprays. For this reason, it is important to measure these parameters during an experiment. It is also important to measure the parameters which may change as the droplet diameter and oxygen concentration are varied, for example the pressure and temperature in the vessel and the burn rate. By measuring these parameters for each experiment, it is possible to see the changes that occur as the initial conditions are varied. The pressure in the piping, exit velocity, initial sodium temperature, and sodium flow rate must also be well characterized for each experiment to ensure the boundary conditions are well captured.

One technique that can be used to experimentally verify exit velocity is the use of a Phase Doppler Particle Analyzer (PDPA). Spray Systems Co. described a PDPA as a two-dimensional point sampling device and flux-sensitive instrument. It operates by using lasers to target and analyze a particular portion of the spray in order to obtain a distribution. Droplets pass through the intersection of the low powered laser beams and scatter the beam (Spray Systems Co., 2005). “Since the droplet is moving the scattered interference pattern sweeps past the receiver aperture at the Doppler difference frequency, which is proportional to the droplet velocity. The spatial frequency is inversely proportional to the droplet diameter” (Spray Systems Co., 2005). As the exit velocity out of the hole increases, the droplet diameter decreases (Spray Systems Co., 2005). A schematic of the Phase Doppler Particle Analyzer can be seen in Figure 26.

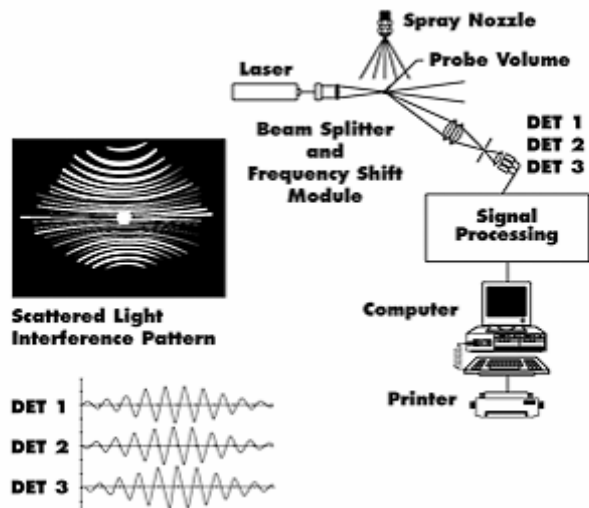


Figure 26 Phase Doppler Particle Analyzer
(Spray Systems Co., 2005)

A brief overview of the instrumentation that may be used in the experiments has been given in Section 4.2. For the purposes of this report, it is not necessary to determine the exact instrumentation or methods used. Instead, potentially important parameters have been identified and the details of measurement will be decided upon by the technical staff at SNL.

4.8. Cleanup Procedures

The proper cleanup and disposal of the equipment and vessel is necessary after each liquid sodium experiment. This procedure is essential because without proper care, residue sodium and residue combustion products can affect the outcome of new experiments or possibly cause a hazardous situation. The following experiments provided information regarding their cleanup procedures that may be helpful in choosing procedures to follow once the experiments have been completed by the SNL staff.

Lancet *et al.* completed spray fire experiments, which can be reviewed in *United States Position Paper on Sodium Fires Design Basis and Testing*. The first concern during the clean up procedures following these experiments was to ensure that all combustible materials were removed safely and quickly from the vessel. Such combustible materials could include unburned sodium or residues. In order to ensure the removal of all combustion products, any sodium, sodium oxide, or other debris were removed from all of the surfaces using chisels and scrapers as

necessary. Once this was complete, each surface was cleaned using a damp sponge or rag. After the vessel surfaces were cleaned, it was necessary to remove the unburned sodium from the collection pan, which was inerted with nitrogen during the first stage of cleanup. This sodium was melted so that it could be removed from the pan with the help of chisels and scrapers (Lancet *et al.*, 1988). Once the catch pan was cleaned, every piece of equipment or hardware involved in the experiment was “misted with water to remove any traces of sodium combustion products” (Lancet *et al.*, 1988).

The second concern was to ensure that all sodium combustion products were disposed of safely and properly. In order to achieve this, “all sodium combustion products were carefully packaged and disposed of as hazardous corrosive waste” (Lancet *et al.*, 1988). All water that was used to rinse or clean the equipment was also disposed of in this way (Lancet *et al.*, 1988).

While this report does not attempt to recommend specific clean up procedures for the experiments conducted at SNL, this section has identified some of the concerns that should be addressed. The procedures chosen should ensure the safety of all personnel involved, as prepare the vessel for following experimental trials.

5. Conclusions and Recommendations

Based on the completed literature search and preliminary experimental design calculations, conclusions and recommendations were formed. The following section describes conclusions regarding the burn rate assumed for the calculations, the leak flow rate calculations, the flow rate and droplet diameter of sodium as compared to that of water calculations, the nozzle choice, and the nozzle height required in order to achieve complete burning.

The burn rate that was assumed for the calculations is the best estimate for the preliminary design of the sodium experiments. At this time, the process of determining the burn rate for a particular falling droplet is done through numerical methods and computer modeling, which may not have been extensively validated. A factor that significantly influences the burn rate of sodium in a spray fire is the availability of oxygen. It may be difficult for the oxygen to penetrate the spray, thus resulting in a lower burn efficiency and the possibility of supplemental sodium pool combustion. Another factor in the burn rate is the influence of the radiative feedback heating between droplets. It is unknown which of these two parameters will have a larger affect on the burn rate due to the limited amount of experimental work in the literature. A wide range of initial experimental parameters should be investigated in order to understand these concepts.

The leak flow rate out of the pipe was calculated based on the pressure difference along the streamline between the inside and the outside of the pipe. As previously stated, the Bernoulli's equation method has many limitations. The flow rate beyond these limitations was approximated using a linear transition from the flow at the limitation point assumed. If flow rates out of larger size holes are of interest, then other methods of calculations should be investigated.

The flow rate of sodium out of a hole will be greater than the flow rate of water, under the same operating conditions, due to the difference in properties between the two fluids. The density of the sodium influences its specific gravity, which specifies the conversion factor between the different fluids. Depending on the operating temperature of the sodium, and thus the density, the flow rate of sodium will be between 1.05 and 1.12 times larger than the flow rate of

water. This is an accurate conversion of flow rates between fluids; however, one must be cautious in understanding the limitations of calculating the sodium flow rate before converting into the flow rate of water.

A similar comparison to the flow rate of sodium and water can be made for the size of the droplets out of a nozzle for the two fluids. The diameter of a droplet calculated was largely dependent on the surface tension and density of the fluid. For any particular operating conditions, the diameter of the sodium droplet will be approximately 2.2 times larger than the diameter of the water droplet. The scaling exercise used resulted in an approximation and cannot be assumed to be exact. Experimental methods should be used to characterize the droplet diameter out of a nozzle if it is a critical parameter for the experiment.

Since the experiments to be conducted by SNL aim to simulate postulated leaks, it was necessary to select an appropriate nozzle. Based on the parameters of the postulated leak scenarios and the need to create a sodium spray that will completely burn before reaching the bottom of the vessel, it was decided that the category of full cone best fit the needs of the experiment. From this category, several specific models from the group named Axial Full Cone Large Capacity Nozzles were selected. These models were chosen because they are able to operate at a range of values that encompasses Scenarios A, B, and C, as well as many other situations (Lechler, 1992).

The required height of the nozzle in order to achieve complete burning of the sodium is dependent on the diameter of the droplets. The nozzle selected to complete the testing will specify this diameter. For the experiments that will occur, it is unknown how much the radiative feedback heating between droplets and oxygen penetration into the spray will influence the burn rate. Thus, the required distance may be affected. To be conservative, the first trials should involve a nozzle that will produce smaller droplets than was calculated in order to ensure complete burning is achieved. Appendix B has suggested heights for numerous scenarios involving sodium at 450 °C and 500 °C.

The findings and calculations completed in this report are recommendations for the experimental design parameters. A clear understanding of the methods, assumptions, and limitations shall be verified before applying them to a particular situation. If a parameter is critical to the experiment and an approximation has been calculated based on the methods presented, it should also be experimentally verified.

References

- Alexandrou, A., 2001, *Principles of Fluid Mechanics*. Prentice-Hall INC., New Jersey.
- Antonakas D., 1988, The Detection of Leaks on Sodium Pipes in a “Leak Before Break” Approach, in *International Working Group Fast Reactors, Specialists’ Meeting Sodium Fires, Session 1*, held in Obninsk, USSR, June 6-9, 1988. International Atomic Energy Agency.
- Babinsky, E., and P.E. Sojka, 2002, Modeling Drop Size Distributions, in *Progress in Energy and Combustion Science*, vol 28, issue 4, pp. 303-329.
- Blanchat, T. K., R. T. Nichols, V. G. Figueroa, 2007, *Benchmark Enclosure Fire Suppression Experiments – Phase 1 Test Report*, SAND2007-3220, Sandia National Laboratories, Albuquerque, NM, June 2007.
- Calvert, J.B., 2003, *Coefficient of Discharge*, 16 January 2008, <<http://mysite.du.edu/~jcalvert/tech/fluids/orifice.htm#Intr>>.
- Cherdron, W., 1986, Experimental Results of Large-Scale Sodium Spray Fires, in *Science and technology of fast reactor safety*, Paper 14, pp. 75-77.
- Cherdron, W., K. Freudenstein, and S. Jordan, 1988, Sodium Fire Research Programs for SNR Safety in FRG, in *International Working Group Fast Reactors, Specialists’ Meeting Sodium Fires, Session 1*, held in Obninsk, USSR, June 6-9, 1988. International Atomic Energy Agency.
- Cherdron W., and S. Jordan, 1988a, Aerosol Release from Sodium Fires and their Consequences for Reactor Components, in *International Working Group Fast Reactors, Specialists’ Meeting Sodium Fires, Session 1*, held in Obninsk, USSR, June 6-9, 1988. International Atomic Energy Agency.
- Cherdron, W., and S. Jordan, 1988b, Thermodynamic Consequences of Sodium Leaks and Fires in Reactor Containments, in *International Working Group Fast Reactors, Specialists’ Meeting Sodium Fires, Session 1*, held in Obninsk, USSR, June 6-9, 1988. International Atomic Energy Agency.
- Government of India, Department of Atomic Energy, 2004, *Sodium Concrete-Interactions Studies*. 9 November 2007 <<http://www.igcar.gov.in/igc2004/sg/concrete.htm>>.
- Gracie, J.D., and J.J. Droher, 1960, *A Study of Sodium Fires*, Atomics International, October 15, 1960.
- Heisler M. P., R. P. Johnson, R. L. Koontz, and D. Toppen, 1975b, Atomics International Report AI-ERDA-13155.

- Heisler M. P., R. P. Johnson, J. M. Otter, C. T. Nelson, E. R. Specht., C. Gunderjahn, and E. U. Vaughan, 1975a, *Atomics International Report AI-ERDA-13161*.
- Hines, E., A. Gemant, and J.K. Kelly, 1956, How Strong Must Reactor Housings Be To Contain Na-Air Reactions, in *Nucleonics*, vol 14, Number 10.
- Himeno, Y., 1988, Current Status of Sodium Fires and Aerosol Research in Japan, in *International Working Group Fast Reactors, Specialists' Meeting Sodium Fires, Session 1*, held in Obninsk, USSR, June 6-9, 1988. International Atomic Energy Agency.
- Incropera, F. P., and D. P. DeWit, 2002, *Introduction to Heat Transfer 4th Edition*. John Wiley and Sons, USA.
- International Working Group Fast Reactors, Specialists' Meeting Sodium Fires, Session 1, 1988, held in Obninsk, USSR, June 6-9, 1988. International Atomic Energy Agency.
- Johnson, R. P., M. Silberberg, J. Hopenfeld, and P. Beiriger, 1968, *Characterization of Sodium Pool Fires*. Proceedings of the International Conference on Sodium Technology and Large Fast Reactor Design, Part I, Sessions on Sodium Technology, Argonne National Laboratory, ANL-7520, pp. 195-205.
- Kawabe, R., A. Suzuoki, A. Minato, N. Sagawa, and S. Sakaguchi, 1982, A Study on Sodium Spray Combustion, in *Nuclear Engineering and Design*, Vol. 75, pp. 49-56, North-Holland Publishing Company.
- Krolikowski, T. S., 1968, *Violently Sprayed Sodium-Air Reaction in an Enclosed Volume*. Wayne State University, Detroit, Michigan.
- Krolikowski T. S., Lebowitz L., Wilson R. E., and Cassulo J. C., 1969, The Reaction of a Molten Sodium Spray with Air in an Enclosed Volume: Part 2 Theoretical Model, in *Nuclear Sci. Eng.*, 38, 161-166.
- Lancet, R. T., R. P. Johnson, E. Matlin, E. U. Vaughan, D. E. Fields, E. Gluekler, J. D. McCormack, C. W. Miller, and D. R. Pederson, 1988, United States Position Paper on Sodium Fires Design Basis and Testing, in *International Working Group Fast Reactors, Specialists' Meeting Sodium Fires, Session 1*, held in Obninsk, USSR, June 6-9, 1988. International Atomic Energy Agency.
- Lechler, 1992, *Industrial Spray Nozzles, Systems and Accessories*, Catalog #130
- Lin, S. P. and R.D. Reitz, 1998, Drop and Spray Formation from a Liquid Jet, in *Annual Review Fluid Mechanics*, vol. 30, pp. 85-105.
- Malet, J. C., 1996, Ignition and Combustion of Sodium – Fire Consequences – Extinguishment and Prevention, in *International Working Group Fast Reactors, Technical Committee Meeting on Evaluation of Radioactive Materials Release and Sodium Fires in Fast*

- Reactors*, held in Ibaraki, Japan, November 11-14, 1996. International Atomic Energy Agency.
- Malet, J.C., C. Casselman, G. Duverger de Guy, R. Rzekiecki, and J. Charpenel, 1981, Potential Results of Spray and Pool Fires, in *Nuclear Engineering and Design*, vol. 68, pp. 195-206, North-Holland Publishing Company.
- Mitra, S. K., and Li X., n.d., *A Comprehensive on Model Spray Formation Process and Probability Distribution of Subsequently Formed Spray Droplets*, University of Victoria Victoria, B.C. Canada.
- Morewitz, H. A., 1979, Sodium Spray Fires, in *Nuclear Engineering and Design*, vol. 42, pp. 123-135. North-Holland Publishing Company.
- Morewitz, H.A., R.P. Johnson, and C.T. Nelson, 1977, Experiments on Sodium Fires and Their Aerosols, in *Nuclear Engineering and Design*, vol. 42, pp. 1-186, North-Holland Publishing Company.
- Nave, C.R., 2005, *Physical Properties of Some Typical Liquids*, 13 February 2008, <<http://hyperphysics.phy-astr.gsu.edu/Hbase/hframe.html>>.
- Newman, R. N., 1972, *The Combustion of Liquid Sodium in Air*, Central Generating Electricity Board, Berkeley Nuclear Laboratories.
- Newman, R.N., 1983, The Ignitions and Burning Behavior of Sodium Metal in Air, in *Progress in Nuclear Energy*, Vol. 12, No. 2, pp119-147.
- Newman, R.N. and J. F.P. Payne, n.d., Fundamental Studies of the Mechanism of Sodium Combustion, in *International Conference on Liquid Metal Technology in Energy Production*, Central Generating Electricity Board, Berkeley Nuclear Laboratories.
- Newman, R.N., A.R. Pugh, and C.A. Smith. 1973, Combustion and Explosion Phenomena in Sodium-Water Systems, in *Combustion Institute European Symposium*, held at University of Sheffield, September 16-20, 1973.
- Nowlen, S. P., T. Blanchat, T. J. Olivier, J. Hewson, and R. Radel, n.d., *Metal Fires and Their Implications for Advanced Reactors*, Sandia National Laboratories, Albuquerque, NM.
- Olivier, T., R.F. Radel, S.P. Nowlen, T.K. Blanchat, and J.C. Hewson, *Metal Fire Implications for Advanced Reactors, Part 1: Literature Review*, SAND2007-6332. Sandia National Laboratories, Albuquerque, NM, October 2007.
- Reitz, R. D., and F. V. Bracco, 1982, *Mechanism of Atomization of a Liquid Jet*, Princeton University, Princeton, New Jersey.
- Richard, J.R., R. Delbourgo, and P. Laffitte, 1969, Spontaneous Ignition and Combustion of Sodium Droplets in Various Oxidizing Atmospheres at Atmospheric Pressure, in *Twelfth*

- Symposium (International) on Combustion*, held at University of Poitiers, Poitiers, France, July 14-20,1969.
- Rockwell International, 1975, *Quarterly Technical Progress Report: Nuclear Safety Characterization of Sodium Fires and Fast Reactor Fission Products*, AI-ERDA-13155, Canoga Park, California.
- Serway, R. A., and R. J. Beichner, 2000, *Physics for Scientists and Engineers 5th Ed.* Saunders College Publishing, Philadelphia, Pennsylvania.
- Sorbo, N.W., D.P.Y. Chang, R.R. Steeper, and C.K. Law, 1988, Single Droplet Studies of Surrogate Hazardous Waste Incineration, in *Engineering Evaluation and Control of Toxic Airborne Effluents*, Vol. 1.
- Spraco, Inc., 1983, *Spray Nozzle User's Manual*. Spraco, Inc.
- Spray Systems Company, 2005, *Phase Doppler Particle Analyzers*, 15 January 2008, <<http://www.sprayconsultants.com/pdpa.asp>>.
- TPS, Inc., 2001, *Spray Nozzle Index by Design and Application*, 13 February 2008, <<http://fluidproducts.com/nozzleindex.htm>>.
- Turns, S. R., 2000, *An Introduction to Combustion 2nd Edition*. McGraw-Hill.
- U.S. Department of Energy, Idaho National Laboratory, 2007, *Sodium-Cooled Fast Reactor (SFR)*, 5 November 2007, <<http://nuclear.inl.gov/gen4/sfr.shtml>>.
- U.S. Department of Energy, Global Nuclear Energy Partnership, 2007, *What are Fast Reactors*. 5 November 2007, <<http://www.gnep.energy.gov/pdfs/factSheetPrimerReactors.pdf>>.
- U.S. Department of Energy, Nuclear Energy Research Advisory Committee and the Generation IV International Forum, 2002, *A Technology Roadmap for Generation IV Nuclear Energy Systems*.
- Zung, J. T., 1978, *Evaporation-Combustion of Fuels (Advances in Chemistry Series 166)*. American Chemical Society, Washington D.C.

Appendix A: Scaling Droplet Size Tables

The follow tables contain information used to calculate the difference in droplet size between sodium and water droplets as explained in section 4.3.2. Different leak hole diameters were used to verify that different sizes had no influence on the ratio of droplet diameters expected to be formed by the two fluids.

0.05 m Hole	Water	Sodium
Surf Tension (N/m)	0.072	0.19
Density (kg/m ³)	958	927
Velocity (m/s)	0.02	0.02
R _{water} (m)	6.02E-01	
R _{sodium} (m)	1.31E+00	
R _{Sodium} /R _{water}	2.2	

Table 18: Scaling Droplet Size Calculations for a 50 mm Leak Hole

0.12 m Hole	Water	Sodium
Surf Tension (N/m)	0.072	0.19
Density (kg/m ³)	958	927
Velocity (m/s)	0.09	0.10
R _{water} (m)	1.83E-02	
R _{sodium} (m)	3.97E-02	
R _{Sodium} /R _{water}	2.2	

Table 19: Scaling Droplet Size Calculations for a 120 mm Leak Hole

Appendix B: Required Height for Complete Burn

The following contains the required height necessary for the sodium to be sprayed from in order for complete burning to occur. The tables describe sodium at 450 °C and 500 °C with various injection velocities. The first set of tables corresponds to sodium at 450 °C that have the properties listed in Table 20.

Burn Rate (mg/s)	170
Sodium Density (kg/m ³)	841
Temperature (°C)	450

Table 20: Required Burn Height Properties at 450 °C

Droplet Diameter (mm)	Droplet Volume (m ³)	Mass (mg)	Time to Full Burn (sec)	Required Height for Complete Burn (m)
1	5.2E-10	0.4	0.003	0.003
2	4.2E-09	3.5	0.02	0.02
3	1.4E-08	12	0.1	0.1
4	3.4E-08	28	0.2	0.3
5	6.5E-08	55	0.3	0.8
6	1.1E-07	95	0.6	2.1
7	1.8E-07	151	0.9	4.8
8	2.7E-07	225	1.3	9.9
9	3.8E-07	321	1.9	19
10	5.2E-07	440	2.6	35

Table 21: Required Burn Height with Injection velocity of 1 m/s at 450 °C

Droplet Diameter (mm)	Droplet Volume (m ³)	Mass (mg)	Time to Full Burn (sec)	Required Height for Complete Burn (m)
1	5.2E-10	0.4	0.003	0.01
2	4.2E-09	3.5	0.02	0.04
3	1.4E-08	12	0.1	0.2
4	3.4E-08	28	0.2	0.5
5	6.5E-08	55	0.3	1.2
6	1.1E-07	95	0.6	2.7
7	1.8E-07	151	0.9	5.6
8	2.7E-07	225	1.3	11
9	3.8E-07	321	1.9	21
10	5.2E-07	440	2.6	38

Table 22: Required Burn Height with Injection velocity of 2 m/s at 450 °C

Droplet Diameter (mm)	Droplet Volume (m ³)	Mass (mg)	Time to Full Burn (sec)	Required Height for Complete Burn (m)
1	5.2E-10	0.4	0.003	0.01
2	4.2E-09	3.5	0.02	0.1
3	1.4E-08	12	0.1	0.4
4	3.4E-08	28	0.2	1.0
5	6.5E-08	55	0.3	2.1
6	1.1E-07	95	0.6	4.3
7	1.8E-07	151	0.9	8.3
8	2.7E-07	225	1.3	15
9	3.8E-07	321	1.9	27
10	5.2E-07	440	2.6	46

Table 23: Required Burn Height with Injection velocity of 5 m/s at 450 °C

Droplet Diameter (mm)	Droplet Volume (m ³)	Mass (mg)	Time to Full Burn (sec)	Required Height for Complete Burn (m)
1	5.2E-10	0.4	0.003	0.02
2	4.2E-09	3.5	0.02	0.2
3	1.4E-08	12	0.1	0.6
4	3.4E-08	28	0.2	1.5
5	6.5E-08	55	0.3	3.1
6	1.1E-07	95	0.6	6.0
7	1.8E-07	151	0.9	11
8	2.7E-07	225	1.3	19
9	3.8E-07	321	1.9	33
10	5.2E-07	440	2.6	54

Table 24: Required Burn Height with Injection velocity of 8 m/s at 450 °C

Droplet Diameter (mm)	Droplet Volume (m ³)	Mass (mg)	Time to Full Burn (sec)	Required Height for Complete Burn (m)
1	5.2E-10	0.4	0.003	0.03
2	4.2E-09	3.5	0.02	0.2
3	1.4E-08	12	0.1	0.8
4	3.4E-08	28	0.2	2.0
5	6.5E-08	55	0.3	4.1
6	1.1E-07	95	0.6	7.7
7	1.8E-07	151	0.9	14
8	2.7E-07	225	1.3	23
9	3.8E-07	321	1.9	38
10	5.2E-07	440	2.6	61

Table 25: Required Burn Height with Injection velocity of 11 m/s at 450 °C

Droplet Diameter (mm)	Droplet Volume (m ³)	Mass (mg)	Time to Full Burn (sec)	Required Height for Complete Burn (m)
1	5.2E-10	0.4	0.003	0.04
2	4.2E-09	3.5	0.02	0.3
3	1.4E-08	12	0.1	1.0
4	3.4E-08	28	0.2	2.5
5	6.5E-08	55	0.3	5.0
6	1.1E-07	95	0.6	9.4
7	1.8E-07	151	0.9	16
8	2.7E-07	225	1.3	27
9	3.8E-07	321	1.9	44
10	5.2E-07	440	2.6	69

Table 26: Required Burn Height with Injection velocity of 14 m/s at 450 °C

Droplet Diameter (mm)	Droplet Volume (m ³)	Mass (mg)	Time to Full Burn (sec)	Required Height for Complete Burn (m)
1	5.2E-10	0.4	0.003	0.04
2	4.2E-09	3.5	0.02	0.4
3	1.4E-08	12	0.1	1.2
4	3.4E-08	28	0.2	3.0
5	6.5E-08	55	0.3	6.0
6	1.1E-07	95	0.6	11
7	1.8E-07	151	0.9	19
8	2.7E-07	225	1.3	31
9	3.8E-07	321	1.9	50
10	5.2E-07	440	2.6	77

Table 27: Required Burn Height with Injection velocity of 17 m/s at 450 °C

Droplet Diameter (mm)	Droplet Volume (m ³)	Mass (mg)	Time to Full Burn (sec)	Required Height for Complete Burn (m)
1	5.2E-10	0.4	0.003	0.1
2	4.2E-09	3.5	0.02	0.4
3	1.4E-08	12	0.1	1.4
4	3.4E-08	28	0.2	3.4
5	6.5E-08	55	0.3	7.0
6	1.1E-07	95	0.6	13
7	1.8E-07	151	0.9	22
8	2.7E-07	225	1.3	35
9	3.8E-07	321	1.9	55
10	5.2E-07	440	2.6	85

Table 28: Required Burn Height with Injection velocity of 20 m/s at 450 °C

The next set of tables corresponds to sodium at 500 °C that have the properties listed in Table 29.

Burn Rate (mg/s)	170
Sodium Density (kg/m ³)	829
Temperature (°C)	500

Table 29: Required Burn Height Properties at 500 °C

Droplet Diameter (mm)	Droplet Volume (m ³)	Mass (mg)	Time to Full Burn (sec)	Required Height for Complete Burn (m)
1	5.2E-10	0.4	0.003	0.003
2	4.2E-09	3.5	0.02	0.02
3	1.4E-08	12	0.1	0.1
4	3.4E-08	28	0.2	0.3
5	6.5E-08	54	0.3	0.8
6	1.1E-07	94	0.6	2.0
7	1.8E-07	149	0.9	4.6
8	2.7E-07	222	1.3	9.7
9	3.8E-07	316	1.9	19
10	5.2E-07	434	2.6	34

Table 30: Required Burn Height with Injection velocity of 1 m/s at 500 °C

Droplet Diameter (mm)	Droplet Volume (m ³)	Mass (mg)	Time to Full Burn (sec)	Required Height for Complete Burn (m)
1	5.2E-10	0.4	0.003	0.01
2	4.2E-09	3.5	0.02	0.04
3	1.4E-08	12	0.1	0.2
4	3.4E-08	28	0.2	0.5
5	6.5E-08	54	0.3	1.1
6	1.1E-07	94	0.6	2.6
7	1.8E-07	149	0.9	5.5
8	2.7E-07	222	1.3	11
9	3.8E-07	316	1.9	21
10	5.2E-07	434	2.6	37

Table 31: Required Burn Height with Injection velocity of 2 m/s at 500 °C

Droplet Diameter (mm)	Droplet Volume (m ³)	Mass (mg)	Time to Full Burn (sec)	Required Height for Complete Burn (m)
1	5.2E-10	0.4	0.003	0.01
2	4.2E-09	3.5	0.02	0.1
3	1.4E-08	12	0.1	0.4
4	3.4E-08	28	0.2	0.9
5	6.5E-08	54	0.3	2.1
6	1.1E-07	94	0.6	4.2
7	1.8E-07	149	0.9	8.1
8	2.7E-07	222	1.3	15
9	3.8E-07	316	1.9	26
10	5.2E-07	434	2.6	45

Table 32: Required Burn Height with Injection velocity of 5 m/s at 500 °C

Droplet Diameter (mm)	Droplet Volume (m ³)	Mass (mg)	Time to Full Burn (sec)	Required Height for Complete Burn (m)
1	5.2E-10	0.4	0.003	0.02
2	4.2E-09	3.5	0.02	0.2
3	1.4E-08	12	0.1	0.6
4	3.4E-08	28	0.2	1.4
5	6.5E-08	54	0.3	3.1
6	1.1E-07	94	0.6	5.9
7	1.8E-07	149	0.9	11
8	2.7E-07	222	1.3	19
9	3.8E-07	316	1.9	32
10	5.2E-07	434	2.6	52

Table 33: Required Burn Height with Injection velocity of 8 m/s at 500 °C

Droplet Diameter (mm)	Droplet Volume (m ³)	Mass (mg)	Time to Full Burn (sec)	Required Height for Complete Burn (m)
1	5.2E-10	0.4	0.003	0.03
2	4.2E-09	3.5	0.02	0.2
3	1.4E-08	12	0.1	0.8
4	3.4E-08	28	0.2	1.9
5	6.5E-08	54	0.3	4.0
6	1.1E-07	94	0.6	7.6
7	1.8E-07	149	0.9	13
8	2.7E-07	222	1.3	23
9	3.8E-07	316	1.9	37
10	5.2E-07	434	2.6	60

Table 34: Required Burn Height with Injection velocity of 11 m/s at 500 °C

Droplet Diameter (mm)	Droplet Volume (m ³)	Mass (mg)	Time to Full Burn (sec)	Required Height for Complete Burn (m)
1	5.2E-10	0.4	0.003	0.04
2	4.2E-09	3.5	0.02	0.3
3	1.4E-08	12	0.1	1.0
4	3.4E-08	28	0.2	2.4
5	6.5E-08	54	0.3	5.0
6	1.1E-07	94	0.6	9.2
7	1.8E-07	149	0.9	16
8	2.7E-07	222	1.3	27
9	3.8E-07	316	1.9	43
10	5.2E-07	434	2.6	68

Table 35: Required Burn Height with Injection velocity of 14 m/s at 500 °C

Droplet Diameter (mm)	Droplet Volume (m ³)	Mass (mg)	Time to Full Burn (sec)	Required Height for Complete Burn (m)
1	5.2E-10	0.4	0.003	0.04
2	4.2E-09	3.5	0.02	0.3
3	1.4E-08	12	0.1	1.2
4	3.4E-08	28	0.2	2.9
5	6.5E-08	54	0.3	5.9
6	1.1E-07	94	0.6	11
7	1.8E-07	149	0.9	19
8	2.7E-07	222	1.3	31
9	3.8E-07	316	1.9	49
10	5.2E-07	434	2.6	75

Table 36: Required Burn Height with Injection velocity of 17 m/s at 500 °C

Droplet Diameter (mm)	Droplet Volume (m ³)	Mass (mg)	Time to Full Burn (sec)	Required Height for Complete Burn (m)
1	5.2E-10	0.4	0.00	0.1
2	4.2E-09	3.5	0.02	0.4
3	1.4E-08	12	0.1	1.4
4	3.4E-08	28	0.2	3.4
5	6.5E-08	54	0.3	6.9
6	1.1E-07	94	0.6	13
7	1.8E-07	149	0.9	21
8	2.7E-07	222	1.3	34
9	3.8E-07	316	1.9	54
10	5.2E-07	434	2.6	83

Table 37: Required Burn Height with Injection Velocity of 20 m/s at 500 °C

Appendix C: Nozzle Comparison to Scenarios

These tables compare the postulated scenario specification to various models of nozzles within the group Axial Full Cone Large Capacity Nozzles (Lechler, 1992).

	Inside Pressure (kPa gauge)	Orifice Diameter (mm)	Water Flow Rate (kg/s)
Scenario A	100	10	0.69
Nozzle 461.124	70	9.0	0.69
Scenario A	100	20	2.6
Nozzle 461.364	70	18	2.7
Scenario A	100	30	6.0
Nozzle 403.524	70	29	6.9
Scenario A	100	40	11
Nozzle 403.604	70	36	11
Scenario A	100	50	17
Nozzle 403.628	140	42	18

**Table 38: Nozzle Comparison to Scenario A
(Lechler, 1992)**

	Inside Pressure (kPa gauge)	Orifice Diameter (mm)	Water Flow Rate (kg/s)
Scenario B	210	10	0.95
Nozzle 461.124	140	9.0	0.88
Scenario B			
Scenario B	210	20	3.9
Nozzle 461.364	140	18	3.6
Scenario B			
Scenario B	210	30	8.8
Nozzle 403.524	140	29	9.0
Scenario B			
Scenario B	210	40	16
Nozzle 403.604	140	36	14

**Table 39: Nozzle Comparison to Scenario B
(Lechler, 1992)**

	Inside Pressure (kPa gauge)	Orifice Diameter (mm)	Water Flow Rate (kg/s)
Scenario C	20	9.9	0.32
Nozzle 461.124	35	9.0	0.50
Scenario C			
Scenario C	20	20	1.3
Nozzle 461.364	35	18	2.1
Scenario C			
Scenario C	20	30	2.8
Nozzle 461.404	35	20	2.6
Scenario C			
Scenario C	20	40	4.9
Nozzle 403.524	35	29	5.2
Scenario C			
Scenario C	20	50	7.8
Nozzle 403.604	35	36	8.3


**Table 40: Nozzle Comparison to Scenario C
(Lechler, 1992)**

Nozzle Model	Scenario A	Scenario B	Scenario C
461.124	Yes	Yes	Yes
461.364	Yes	Yes	Yes
403.524	Yes	Yes	Yes
403.604	Yes	Yes	Yes
403.628	Yes	No	No
461.404	No	No	Yes

**Table 41: Summary of Nozzle Comparison
(Lechler, 1992)**

Appendix D: Presentation to SNL



The following presentation was given to the technical staff at SNL.



Studies of Metal Fires

Study of Sodium Spray Fires for Sandia National Laboratories




Robert Accosta
Laura Archer



Outline

- **Background research**
- **Experiment overview**
 - Leak flow calculations
 - Spray patterns
 - Burn rate
 - Required nozzle height for complete burn
 - Nozzle selection
- **Conclusions**
- **Recommendations**

2





Background Research

- Importance of sodium
- Sodium properties
- Pool combustion
- Spray combustion
 - Theoretical
 - Experimental

3

Worcester Polytechnic Institute



Experiment Overview

- Experiments to be performed in Surtsey vessel
- Spray, pool, and combination experiments to be conducted

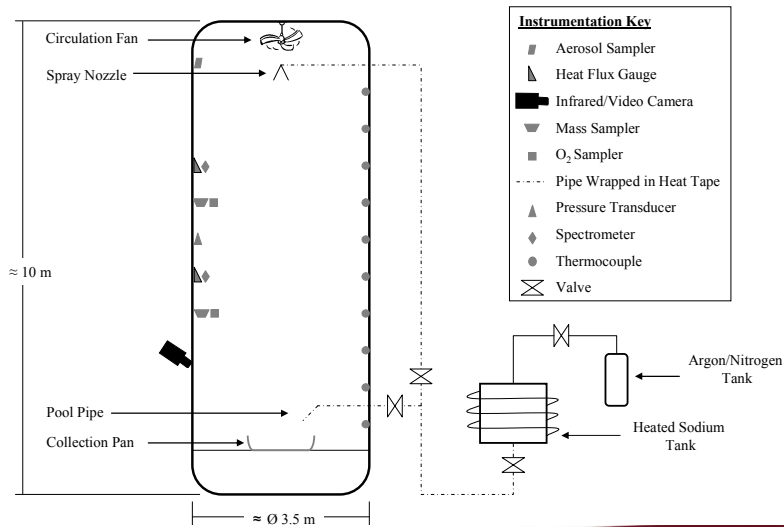


4

Worcester Polytechnic Institute



Cross Section of Vessel



5

Worcester Polytechnic Institute



Design Assumptions

- Leak will be through a circular hole
- Hole diameter remains constant
- Pipe is not jacketed, but thermally insulated

6

Worcester Polytechnic Institute





Postulated Leak Scenarios

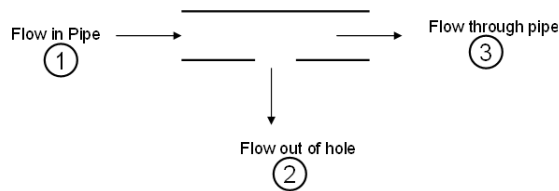
	Scenario A	Scenario B	Scenario C
Density (kg/m ³)	830	870	870
Temperature (°C)	488	326	333
Absolute Pressure Inside Pipe (kPa)	200	300	120
Absolute Pressure Outside Pipe (kPa)	101	101	101
Pipe Mass Flow Rate (kg/s)	628	645	21.5
Pipe Inside Diameter (m)	0.38	0.38	0.38

7

Worcester Polytechnic Institute



Scenario Sodium Leak Flow



- **Bernoulli's equation along a streamline**
 - Given P_1 , P_2 , and V_1
 - Assumed P_3 and V_3
- **Calculated V_2**

8

Worcester Polytechnic Institute





Scenario Sodium Leak Flow

Assumed flow is steady, isothermal, and adiabatic

$$\frac{d}{dt} \int_{V_{\text{os}}} \left(\frac{V^2}{2} + gz + u \right) \rho dV + \int_{A_r} \rho \left(h + \frac{V^2}{2} + gz \right) \vec{V} \cdot \vec{n} dA_r = \dot{Q} - \dot{W}$$

$$\hookrightarrow \left(\frac{P}{\rho} + gz + \frac{V^2}{2} \right)_1 = \left(\frac{P}{\rho} + gz + \frac{V^2}{2} \right)_2 = \text{const.}$$

$$\hookrightarrow V_{\text{out}} = C_D \sqrt{\frac{2(P_{\text{in}} - P_{\text{out}})}{\rho}}$$

9



Scenario Sodium Leak Flow

- Calculated velocities

	Scenario A	Scenario B	Scenario C
Leak Velocity (m/s)	9.5	13	4.1

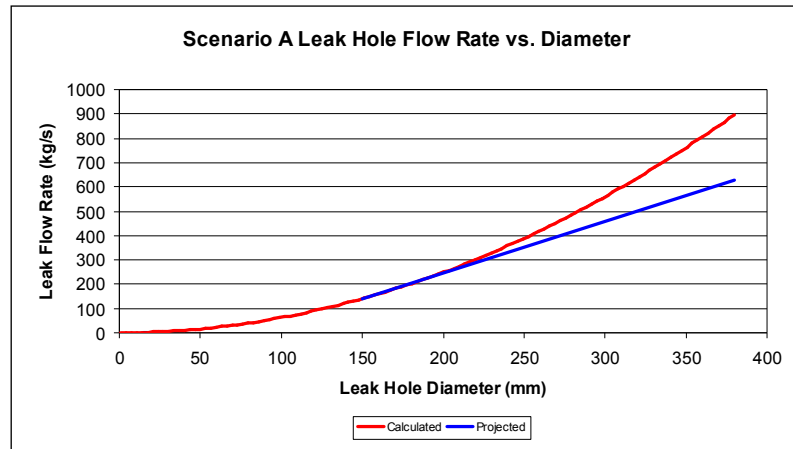
- Calculated mass flow rates (kg/s)

Hole Diameter (mm)	Scenario A	Scenario B	Scenario C
1	0.01	0.01	0.003
5	0.2	0.2	0.1
10	0.6	0.9	0.3
20	2.5	3.6	1.1
30	5.6	8.1	2.5
40	10	14	5
50	16	22	7
60	22	32	10

10



Scenario Sodium Leak Flow



11

Worcester Polytechnic Institute



Water Flow Rate Comparison

- Match specific gravity to conversion factor
 - Scenario A: CF=1.12
 - Scenario B & C: CF=1.05
- Calculate flow rate of water

$$\dot{Q}_w = \frac{\dot{Q}_s}{CF}$$

Diameter of Hole (mm)	Scenario A (kg/s)		Scenario B (kg/s)		Scenario C (kg/s)	
	Sodium	Water	Sodium	Water	Sodium	Water
1	0.01	0.01	0.01	0.01	0.003	0.003
5	0.2	0.1	0.2	0.2	0.1	0.1
10	0.6	0.6	0.9	0.9	0.3	0.3
20	2.5	2.2	3.6	3.4	1.1	1.1
30	5.6	5.0	8.1	7.7	2.5	2.4
40	10	8.9	14	14	4.5	4.3
50	16	14	22	21	7.1	6.7
60	22	20	32	31	10	9.7

12

Worcester Polytechnic Institute

(Spraco, Inc., 1983)





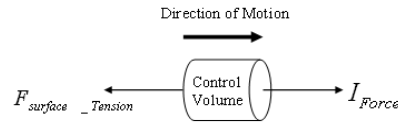
Sodium Droplet Comparison

- **Surface tension force**

$$F_{\text{surface_Tension}} = 2\pi R * \sigma$$

- **Inertial force**

$$I_{\text{Force}} = \rho V^2 L$$



- **Droplets form when balanced**

$$R = \frac{2\sigma}{\rho V^2} \quad \longrightarrow \quad \text{Ratio} = \frac{R_{\text{Sodium}}}{R_{\text{Water}}} \quad \longrightarrow \quad \text{Ratio} = 2.2$$

13



Spray Patterns

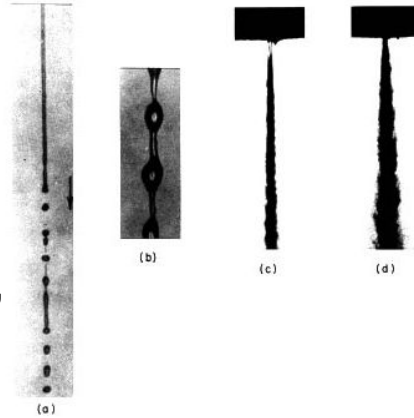
- **Spray patterns**
 - Categorized into four regimes
 - Effected by hole size and exit velocity
 - Defined by the Weber number
- **Droplet diameter distribution**
 - Unknown for first three regimes
 - Three methods of atomization

14

Spray Patterns

Regimes:

- (a) Rayleigh
 $We < 0.4$
- (b) 1st wind-induced,
 $0.4 < We < 13$
- (c) 2nd wind-induced,
 $13 < We < 40.3$
- (d) Atomization,
 $We > 40.3$



15

Spray Formation Calculations

Hole Diameter (mm)	Scenario A		Scenario B		Scenario C	
	Weber Number	Breakup Regime	Weber Number	Breakup Regime	Weber Number	Breakup Regime
10	4.4	1st wind-ind.	8.3	1st wind-ind.	0.8	1st wind-ind.
20	8.7	1st wind-ind.	17	2nd wind-ind.	1.6	1st wind-ind.
30	13	2nd wind-ind.	25	2nd wind-ind.	2.4	1st wind-ind.
40	18	2nd wind-ind.	33	2nd wind-ind.	3.3	1st wind-ind.
50	22	2nd wind-ind.	42	Atomization	4.1	1st wind-ind.
60	26	2nd wind-ind.	50	Atomization	4.9	1st wind-ind.

$$We_g = \frac{\rho_2 U^2 (2a)}{\sigma}$$

16



Burn Rate

- Stationary droplet limited by heat transfer

$$Br = r \left[9.95 * 10^{-2} \left(\frac{T}{573} \right)^{1.75} X_{O_2} - 2.12 * 10^{-3} \right]$$

- Droplet subjected to free convection

$$B_r = \frac{Sh(D)}{d} C_{mean} (X_{O_2,\infty} - X_{O_2,flame})$$

$$Sh = 2 + 0.43(Gr)^{1/4} (Sc)^{1/3}$$

- Droplet subjected to forced convection

“the burning rate of sodium in 21 % O₂ was 170 mg/s”

17



Required Nozzle Height for Complete Burn

Assumptions

- Constant density
- Constant burn rate = 170 mg/s
- Droplet remains a perfect sphere

$$V_{sphere} = \frac{4}{3} \pi r^3$$

$$\hookrightarrow m = \rho V$$

$$\hookrightarrow t_{complete_burn} = \frac{m}{Br}$$

$$\hookrightarrow \Delta Y = v_{y_0} t + \frac{1}{2} a_y t^2$$

18



Required Nozzle Height for Complete Burn

	Scenario A	Scenario B	Scenario C
Sodium Density (kg/m ³)	830	870	870
Initial Velocity (m/s)	9.5	13	4.1

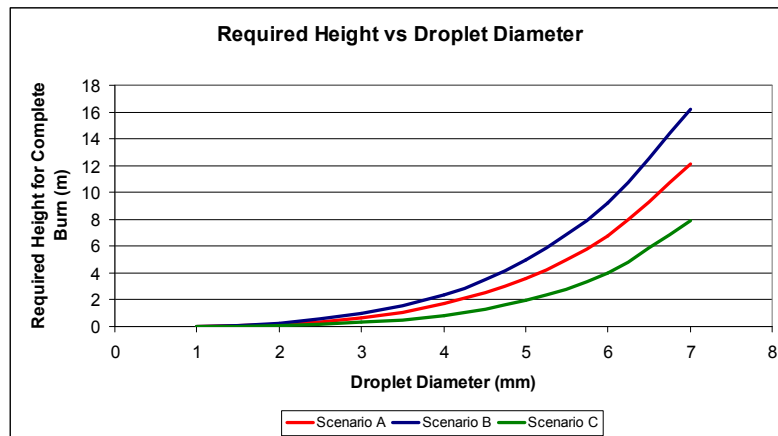
Droplet Diameter (mm)	Required Height for Complete Burn (m)		
	Scenario A	Scenario B	Scenario C
1	0.02	0.04	0.01
2	0.2	0.3	0.1
3	0.7	1.0	0.3
4	1.7	2.4	0.9
5	3.6	4.9	1.9
6	6.8	9.2	4.0
7	12	16	8

19

Worcester Polytechnic Institute



Required Nozzle Height for Complete Burn



20

Worcester Polytechnic Institute





Required Nozzle Height for Complete Burn

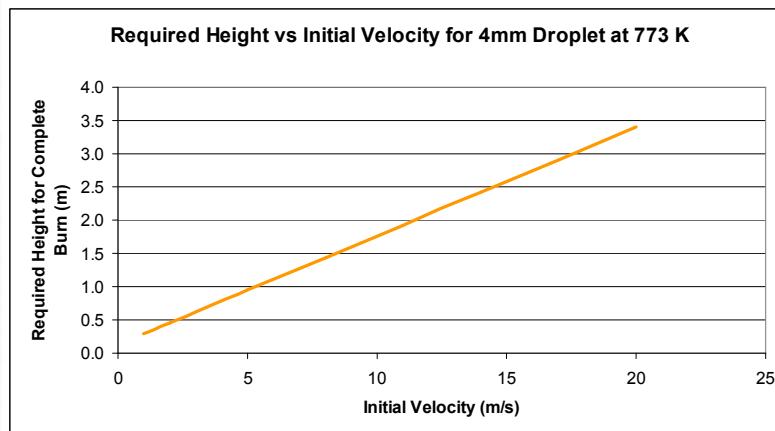
Droplet Diameter (mm)	Required Height for Complete Burn (m)				
	V = 1 m/s	V = 5 m/s	V = 11 m/s	V = 17 m/s	V = 20 m/s
1	0.003	0.01	0.03	0.04	0.05
2	0.02	0.1	0.2	0.3	0.4
3	0.1	0.4	0.8	1.2	1.4
4	0.3	0.9	1.9	2.9	3.4
5	0.8	2.1	4.0	5.9	6.9
6	2.0	4.2	7.6	11	13
7	4.6	8.1	13	19	21

21

Worcester Polytechnic Institute



Required Nozzle Height for Complete Burn



22

Worcester Polytechnic Institute





Nozzle Selection

- Attempt to simulate a postulated leak
- Operate with postulated pressure, outlet diameter, and flow rate
- Consider droplet diameter produced to be more important consideration
- Choose either flat fan, full cone, hollow cone, or atomization nozzle

23



Nozzle Selection

- Largest water droplet diameter is 2800 μm
- Based on complete burn in less than 10 m
- Full cone is the best choice based on droplet diameter
- Axial full cone large capacity nozzles

Nozzle Category	Droplet Description	Approximate Droplet Diameter of Water (m)
Flat Fan	fine	40 μm to 500 μm
Full Cone	fine to coarse	> 500 μm
Hollow Cone	fine	40 μm to 500 μm
Atomization	fine to very fine	10 μm to 40 μm

24



Conclusions: Burn Rate

- **Best estimate was used for the calculation**
- **Numerical methods and computer models are the current method**
- **Oxygen penetration into spray and radiative feedback affect the burn rate**

25

Worcester Polytechnic Institute



Sandia
National
Laboratories



Conclusions: Leak Flow Rate

- **Based on pressure difference**
- **Predicted flow rate using linear transition**
- **Many limitations to this method**
- **Sodium flow rate compared to water**
 - **Difference in physical properties affect the flow rate**
 - **Specific gravity drives the conversion factor**

26

Worcester Polytechnic Institute



Sandia
National
Laboratories





Conclusions: Droplet Size

- **Scaling between liquid properties**
- **Sodium droplet 2.2 times larger than a water droplet**
- **Required height for complete burn**
 - **Dependent on droplet diameter, oxygen penetration, radiative feedback, and burn rate**

27

Worcester Polytechnic Institute



Recommendation

The presented calculations are a recommendation for experimental design parameters

28

Worcester Polytechnic Institute





Acknowledgements

Our project would not have been possible without the help and support of many individuals:

- Professor Tryggvason (WPI)
- Tara Olivier
- Thomas Blanchat
- Jeffrey Danneels
- John Hewson
- Steven Nowlen

29

Worcester Polytechnic Institute



References

- Alexandrou, A., 2001, *Principles of Fluid Mechanics*. Prentice-Hall INC., New Jersey.
- Lechler, 1992, *Industrial Spray Nozzles, Systems and Accessories*, Catalog #130
- Lin, S. P. and R.D. Reitz, 1998, Drop and Spray Formation from a Liquid Jet, in *Annual Review Fluid Mechanics*, vol. 30, pp. 85-105.
- Newman, R.N., 1983, The Ignitions and Burning Behavior of Sodium Metal in Air, in *Progress in Nuclear Energy*, Vol. 12, No. 2, pp119-147.
- Olivier, T.J., R.F. Radel, S.P. Nowlen, T.K. Blanchat, J.C. Hewson. Metal Fire Implications for Advanced Reactors, Part 1: Literature Review. SAND07-6332. Albuquerque, NM: Sandia National Laboratories, 2007.
- Rockwell International. 1975, *Quarterly Technical Progress Report: Nuclear Safety Characterization of Sodium Fires and Fast Reactor Fission Products*, AI-ERDA-13155, Canoga Park, California.
- Sorbo, N.W., D.P.Y. Chang, R.R. Steeper, and C.K. Law, 1988, Single Droplet Studies of Surrogate Hazardous Waste Incineration, in *Engineering Evaluation and Control of Toxic Airborne Effluents*, Vol. 1.
- Spraco, Inc., 1983, *Spray Nozzle User's Manual*. Spraco, Inc.
- TPS, Inc., 2001, *Spray Nozzle Index by Design and Application*, 13 February 2008, <<http://fluidproducts.com/nozzleindex.htm>>.

30

Worcester Polytechnic Institute



Questions?



31

Worcester Polytechnic Institute



WPI

Appendix E: Breakdown of Contributions

While the following list shows the student who was the main drafter of each section, both students revised and reworked each section throughout the course of the project.

Acknowledgements.....	Laura
Abstract.....	Laura
Executive Summary	Laura
1. Introduction	Robert
2. Background Research	
2.1. Sodium Fast Cooled Reactors.....	Robert
2.2. The Importance of Sodium Fires	Joint
2.3. The Combustion of Sodium	
2.3.1. Properties of Sodium	Robert
2.3.2. Reactions.....	Robert
2.3.3. Pool Fires	Laura
2.3.4. Aerosols	Laura
2.3.5. Spray Fires.....	Robert
2.4. Computer Model Development	Robert
3. Spray Fires	
3.1. Theoretical Combustion	
3.1.1. Single Droplet Combustion.....	Robert
3.1.2. Spray Fires	Laura
3.2. Experimental Combustion	
3.2.1. Single Droplet Experiments.....	Laura
3.2.2. Maximum Pressure Based on Oxygen Concentration	Robert
3.2.3. Upright Nozzles	Robert
3.2.4. Previous Experiments Postulating Realistic Leaks.....	Laura
3.2.5. Previous Experiments Conclusions.....	Joint
3.3. Modeling Drop Size Distributions in Atomized Jets.....	Robert
3.4. Sodium Burn Rate	Robert
4. Preliminary Experiment Design	
4.1. Design Assumptions.....	Laura
4.2. Experiment Overview.....	Joint
4.3. Scenario Leak Flow Calculations.....	Robert
4.3.1. Sodium Flow from a Nozzle as Compared to Water	Laura
4.3.2. Sodium Droplet Diameter as Compared to Water	Robert
4.4. Spray Formation.....	Laura
4.5. Necessary Nozzle Height for Complete Burning	Robert
4.6. Nozzle Selection.....	Laura
4.7. Measurement Techniques.....	Joint
4.8. Cleanup Procedures.....	Laura
5. Conclusions and Recommendations.....	Robert
References.....	Laura
Appendix A: Scaling Droplet Size Tables	Robert
Appendix B: Required Height for Complete Burn	Robert
Appendix C: Nozzle Comparison to Scenarios.....	Laura
Appendix D: Presentation to SNL	Joint